sciendo
Austrian Journal of Earth Sciences | Vienna | 2023 | Volume 116 | 85–107 | DOI: 10.17738/ajes.2023.0004

Organic geochemistry and petrography of Miocene ombrotrophic coals in the tropical Asem-Asem Basin (Kalimantan, Indonesia): Comparison to coeval subtropical coals in the Eastern Alps

Hafidz Noor Fikri[1,2], Reinhard F. Sachsenhofer[1*], Achim Bechtel[1] & Doris Gross[1]

1) Department Applied Geosciences and Geophysics, Montanuniversitaet Leoben, 8700 Leoben, Austria

2) Department of Mining Engineering, Lambung Mangkurat University, Banjarmasin, South Kalimantan, Indonesia

*) Corresponding author: reinhard.sachsenhofer@unileoben.ac.at

KEYWORDS: ombrotrophic peat, basinal mire, climate, Borneo, tropical, subtropical

Abstract

The middle Miocene Warukin Formation in the Asem-Asem Basin (Kalimantan) contains a 20-m-thick coal seam (BL1) that is mined at the Jumbang mine. The seam, formed in a tropical peat, was studied to reconstruct the peat-forming environment and to compare its characteristics with those of similarly aged tropical coals from the Tutupan mine in the Barito Basin (Kalimantan) and similarly aged (~15 Ma) subtropical coal from the Leoben Basin in the Eastern Alps (Austria). Although all coals were formed in ombrotrophic peatlands, the comparison reveals differences in biomarker and maceral composition due to the different climate and flora.

The study is based on 22 coal and three non–coal samples, each representing a stratigraphic interval of 0.2 to 1.0 m. The samples were analyzed for ash yield, carbon and sulphur contents, and maceral composition. Organic geochemical parameters were obtained on eight coal samples to obtain information on the peat-forming vegetation. The low-ash, low-sulphur BL1 seam was deposited in an ombrotrophic basinal (coastal) mire. Locally increased sulphur contents in the lower coal bench BL1L demonstrate brackish influence and a near-shore environment. The vegetation was dominated by angiosperms including abundant dammar resin producing *Dipterocarpaceae*, while the contribution of gymnosperms was negligible.

The Tutupan seams T110 and T210, which were formed in kerapah (inland) ombrotrophic mires, have similar ash yields and sulphur contents but contain higher, although still low, concentrations of gymnosperm-derived diterpenoids. In addition, lower amounts of cadinane-type biomarkers and resinite suggest that *Dipterocarpaceae* were less dominant in kerapah peats. While differences between tropical coals from Kalimantan are minor, major differences exist between the tropical coals and the subtropical ombrotrophic Leoben coal. These include significantly higher concentrations of gymnosperm-derived biomarkers in subtropical peat, lower amounts of resinite due to the absence of *Dipterocarpaceae*, as wells as lower amounts of leaf- and rootlet-derived macerals. Apparently, fungal activity was also reduced in the subtropical Leoben peat. Surprisingly, the average amount of oxidized plant remains is also lower in the subtropical peat.

1. Introduction

Coal is an abundant and relatively cheap fuel, but its combustion produces huge amounts of the greenhouse gas carbon dioxide. In 2021, CO_2 emissions from coal combustion reached an all-time high of 15.2 gigatonnes (Gt) contributing about 40 % of the entire energy-related CO_2 emissions (36.3 Gt; IEA, 2022). Similarly, coal production in 2021 (8173 million tonnes [Mt]) was close to the all-time high reached in 2013 (8256 Mt; BP, 2022). Following China (4126 Mt) and India (811 Mt), Indonesia is the third largest producer of coal (614 Mt) equivalent to 7.5 % of world production. Most of Indonesia's coal reserves are located in Cenozoic basins on the islands of Sumatra and

Kalimantan (Indonesian part of Borneo) (Friederich et al., 2016; Fig. 1).

While coal combustion poses a significant threat to global climate, coal is an excellent archive for reconstructing terrigenous depositional settings. Important statements on the peat-forming environments (e.g., ombrotropic [raised] vs. rheotrophic [low-lying] mire; brackish influence) are possible based solely on basic coal parameters such as seam geometry, ash yield and sulphur content (e.g., Gruber and Sachsenhofer, 2001). Palynological

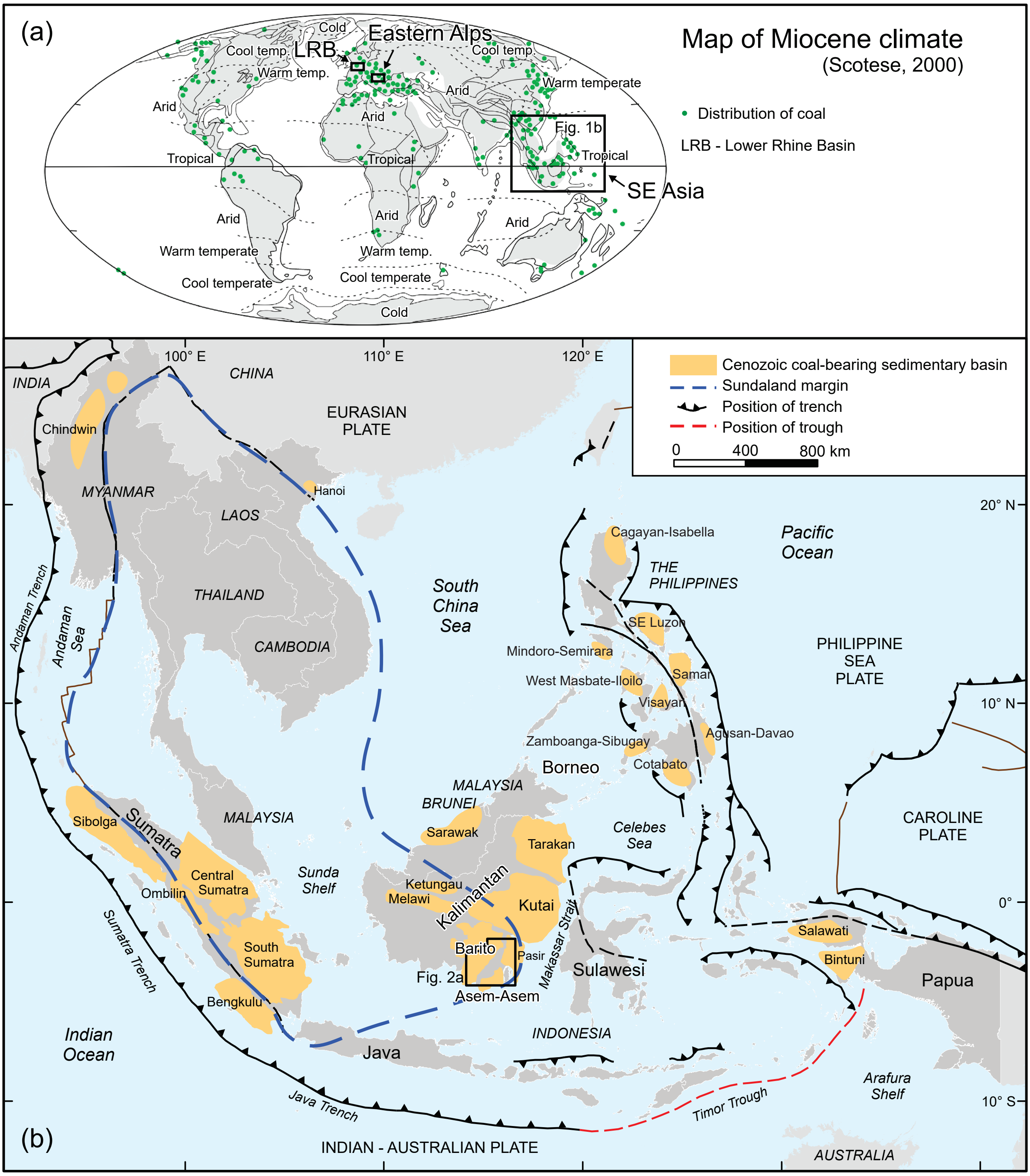

Figure 1: (a) Map of Miocene climate with position of coal deposits (from Scotese, 2000). The locations of Southeast Asia, the Eastern Alps and the Lower Rhine Basin are indicated. **(b)** The main on-shore Cenozoic coal-bearing basins in Southeast Asia (from Friederich et al., 2016).

studies are often used to reconstruct paleovegetation (e.g., Demchuk and Moore, 1993; Rich, 2015; Korasidis et al., 2016; Dai et al., 2020). Petrographic and geochemical parameters provide additional information on the depositional environment and diagenetic processes (e.g., Bechtel et al., 2003a; 2007; 2008; Naafs et al., 2019).

Peat-forming environments of Upper Eocene and middle Miocene coals in the Barito Basin (southern Kalimantan; for location see Figs. 1, 2) were studied recently by Fikri et al. (2022a, b) using bulk geochemical parameters, biomarker and maceral data. Eocene coal seams in the Tanjung Formation from the Tanjung Alam Jaya (TAJ) Pit 1-D mine are 1.4 to 3.4 m thick and originated in rheotrophic low-lying mires dominated by palm and fern vegetation (Fikri et al., 2022b). In contrast, Miocene coal seams in the Warukin Formation from the Tutupan mine are up to 50 m thick and were deposited predominantly in ombrotrophic raised mires (Fikri et al., 2022a). In addition, Miocene coal seams in the Warukin Formation display a remarkable cyclic structure.

In the present study, we investigate a 20-m-thick coal seam in the Warukin Formation (BL1) exposed in the Jumbang open pit mine in the Asem-Asem Basin. The Asem-Asem Basin, located near the southern tip of Kalimantan Island, is considered a sub-basin of the larger Barito Basin, from which it is separated today by the Meratus Complex (Witts et al., 2014; Fig. 2). Similar to Tutupan, coal from the Jumbang mine has very low ash yields (5.5 wt.% adb) and total sulphur contents (0.4 wt.% adb) (Bumi Resources, 2021) making deposition in an ombrotrophic mire likely. The calorific value of Jumbang coal is about 4,200 Kcal/kg (as received, ar) and the average total moisture ~35 wt.% (ar) (Arutmin, 2015). Thus, the coal is classified as lignite.

The paper has three main objectives: (1) reconstruction of environmental conditions during the accumulation of the BL1 seam; (2) comparison of Miocene peat forming conditions in the Asem-Asem Basin (Jumbang mine) and in the Barito Basin (Tutupan mine); and (3) comparison of the characteristics of Miocene ombrotrophic coals from tropical and subtropical regions to investigate the effects of climate on maceral and biomarker compositions.

For this comparison, middle Miocene coals from Kalimantan and from the Leoben Basin in the Eastern Alps of Central Europe are used (Fig. 1a; Gruber and Sachsenhofer, 2001). A considerable number of Miocene coal deposits in the Eastern Alps were formed under subtropical conditions (e.g., Weber and Weiss, 1983), but only the coal in the Leoben Basin was deposited in an ombrotrophic mire (Bechtel et al., 2001; Gruber and Sachsenhofer, 2001; Sachsenhofer et al., 2003).

2. Geological setting

The Asem-Asem Basin is located at the eastern margin of Sundaland, the southeastern promontory of Eurasia (Fig. 1b; Hall and Morley, 2004; Pubellier and Morley, 2014). Sundaland was formed by Permian and Triassic amalgamation of continental blocks and arc fragments (Hutchison, 1989; 2014; Hall and Morley, 2004; Advokaat et al., 2018). Other fragments of oceanic, arc and continental origin accreted to Sundaland during the Cretaceous (e.g., Hall, 2012) and formed the southwestern part of Borneo. The Meratus Complex in southern Borneo (Fig. 2) is interpreted as a Cretaceous subduction complex, which forms the suture between SW Borneo and East Java-West Sulawesi (e.g., Hall, 2012; Witts et al., 2014). An extensional regime was initiated in eastern Borneo by the rifting of the Makassar Strait in the Eocene (e.g., Pubellier and Morley, 2014; Zahirovic et al., 2014; for location

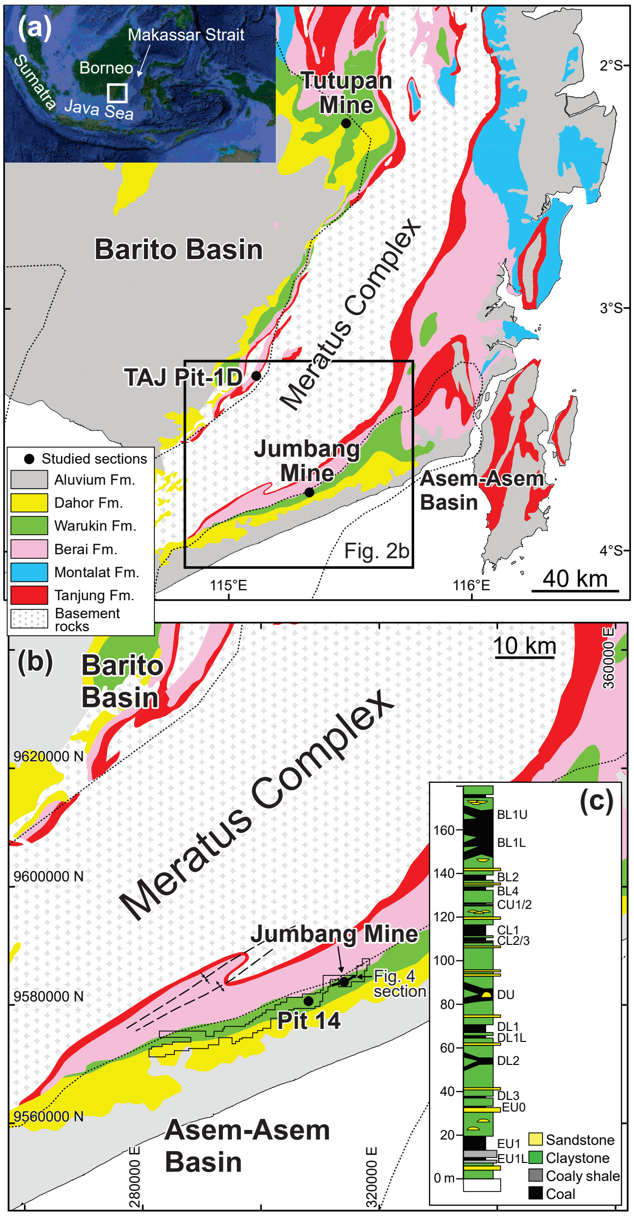

Figure 2: (a) Geological map of the Barito and Asem-Asem basins showing the location of the study site (Jumbang mine) and mines with Eocene (TAJ Pit-1D) and Miocene coals (Tutupan) studied in companion papers (Fikri et al., 2022a, b). **(b)** Geological map of the Asem-Asem Basin showing the location of the study site and the position of the cross-section shown in Figure 4. **(c)** Profile through the Warukin Formation in the study area with seam names (from Achmad, 2018).

see Fig. 1). This extensional event led to the formation of NW-SE oriented horst and graben structures along a succession of NW-SE trending strike-slip faults (Satyana et al., 1999). Rifting ended towards the end of the Early Oligocene (Pubellier and Morley, 2014). Basin inversion commenced in the middle Miocene, around the time of the uplift of the Meratus Mountains (Satyana et al., 1999; Witts et al., 2014).

The Cenozoic basin fill in the Barito Basin and the Asem-Asem Basin is comparable, suggesting that they once formed a uniform depocenter (Witts et al., 2014). The basin fill overlies Cretaceous and older basement rocks unconformably and comprises, from base to top, the Middle Eocene to Lower Oligocene Tanjung Formation, the Upper Oligocene to lower Miocene Berai and Montalat Formations, the middle to upper Miocene Warukin Formation, and the upper Miocene to Pleistocene Dahor Formation (Witts et al., 2012; 2014; Fig. 3). Coal seams occur in the Tanjung Formation and in the Warukin Formation (Friederich et al., 2016). The transgressive Tanjung Formation starts with alluvial and fluvial plain deposits filling a pre-existing relief (Mangkook Member) and continues with fluvio-tidal and estuarine deposits containing several-m-thick and laterally extensive coal seams (Tambak Member). The upper part of the Tanjung Formation consists of marginal to shallow marine rocks dominated by calcareous mudstones (Pagat Member; Witts et al., 2012). The Tanjung Formation is overlain by shallow marine carbonates (Berai Formation) in the Asem-Asem Basin and the southern Barito Basin, and by fluvio-deltaic strata in the northern Barito Basin (Montalat Formation). The regressive Warukin Formation comprises marginal marine rocks with thin coal seams (typically <2 m; Sapiie and Rifiyanto, 2017) in its lower part (Barabai Member of Witts et al., 2012). The overlying Tapin Member (Witts et al., 2012) represents (south-)eastward prograding fluvio-deltaic sedimentary rocks with thick coal seams (Satyana et al., 1999; Witts et al., 2012). A change in paleocurrent directions during deposition of the uppermost part of the Tapin Member in the Barito Basin indicates the middle/late Miocene onset of uplift of the southern part of the Meratus Complex (Witts et al., 2014). In contrast, paleocurrent directions in the Asem-Asem Basin remained southeastward (Witts et al., 2014). Regression and basin inversion continued during deposition of the Dahor Formation (Witts et al., 2014), which consists mainly of alluvial to shallow marine reddish sandstone, polymict conglomerate, and siltstone (Sapiie and Rifiyanto, 2017). In the Asem-Asem Basin, coal seams are locally present in the lower part of the Dahor Formation (Arutmin, 2015).

A significant number of coal seams grouped into seam groups are present in the Warukin Formation in the Asam-Asam Basin. Near the study area the seam groups are labelled from top to bottom with A to E (Fig. 2b). Individual seams are identified by an addition (U for "upper", L for "lower"). The most important seam in the Jumbang mine is seam BL1, which reaches a thickness of 20 m and

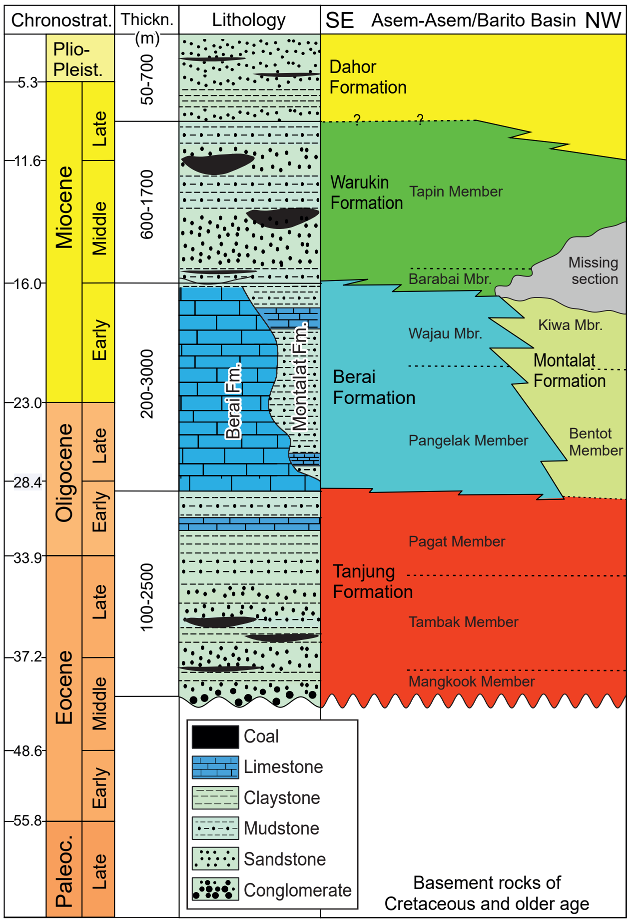

Figure 3: Stratigraphy and lithology of the basin fill in the Asem-Asem Basin (modified after Witts et al., 2012; 2014).

dips gently (6–14°) towards the southeast (125°). A southwest-northeast trending cross-section of the BL1 seam is shown in Figure 4 based on data from exploration boreholes provided by the mine. It shows that the BL1 seam is split into individual coal benches, labelled BL1U and BL1L. Seams A1 and A2 are present with an average thickness of 1.6 m. Seam D2 has an average thickness of 4 m, while seam C2 is thin and discontinuous. The seams are separated by prevailing mudstones and subordinate sandstone beds. The sediments overlying the BL1 seam in the Pit 14 (see Fig. 2b for location) represent floodplain, fluvial channel-belt, estuarine and tidal flat settings (Achmad, 2018). Sediment transport was directed southeastwards (107–160°; Achmad, 2018).

3. Material and methods

Samples were collected at the Jumbang mine (Fig. 2b). At the sampling site, the BL1 seam is 19.4 m thick. Samples were taken from the deposits below and above the seam (2 mudstone samples) and from the seam (22 coal samples, 1 mudstone parting). The samples represent a continuous series of channel samples. Megascopically distinct coal layers were taken separately. Consequently,

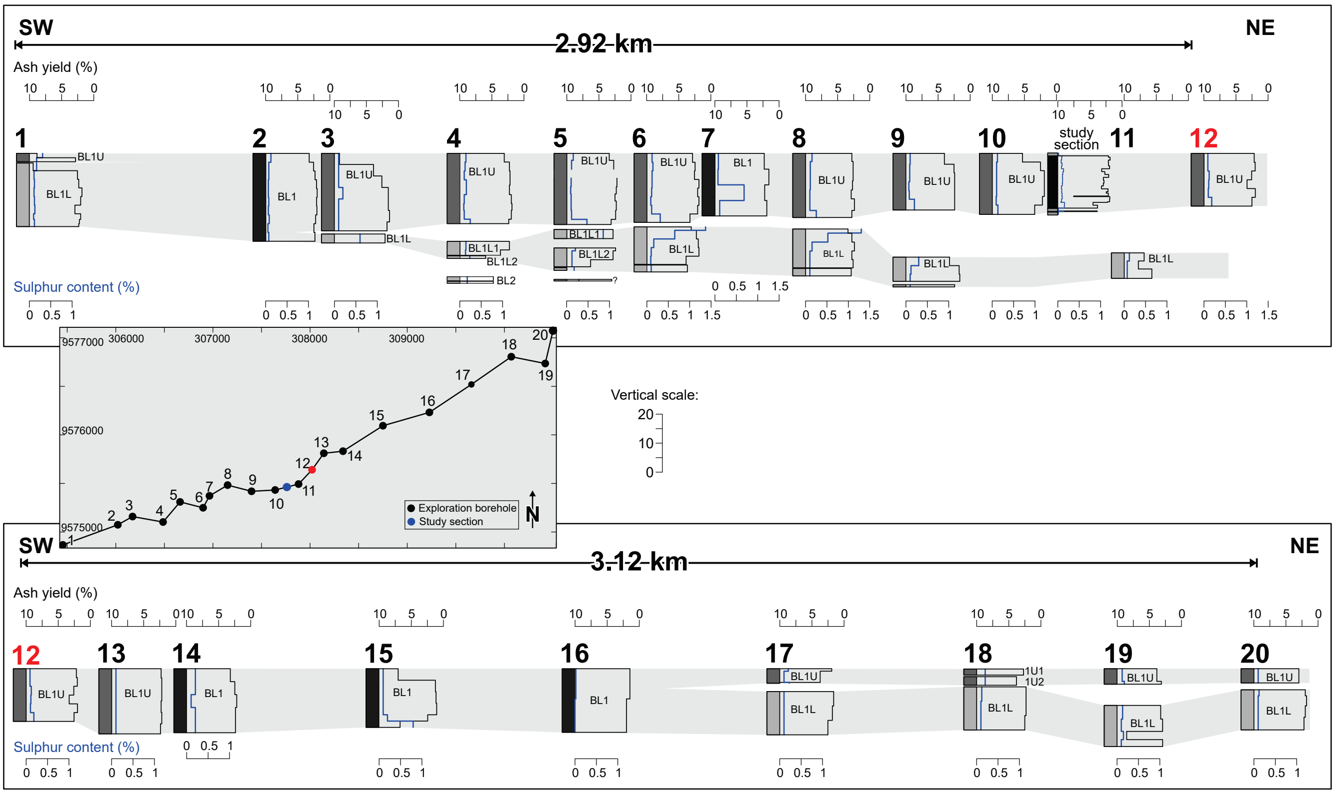

Figure 4: Southwest-northeast trending cross section of the BL1 seam in the Jumbang open pit showing thickness, ash yield (black line) and sulphur content (blue line). Laterally, the BL1 seam splits into an upper (BL1U) and a lower (BL1L) coal bench. The location of the profile is indicated in the inset and in Figure 2b. The profile was compiled using data from exploration boreholes and flattened to the top of the BL1 seam. Position and data from the section studied in the present paper (between boreholes 10 and 11) are shown.

channel samples in the more diverse lower part of the seam (0–7.9 m) are only 0.2 to 1 m long, whereas in the more homogenous upper part of the seam (7.9–19.4 m) they are typically 1 m long. Fresh samples were placed in gas–tight plastic bags immediately after collection to prevent moisture loss.

Samples were prepared at the Mineral and Coal Laboratory of the Mining Department of the Faculty of Engineering (Lambung Mangkurat University). Ash yield and moisture analyses were conducted at the PT Geoservices coal laboratory (Banjarbaru, South Kalimantan) using standard procedures (ASTM, 2012; 2017). Ash yield provides valuable information on peat type (Moore and Shearer, 1997). All other analyses were carried out at Montanuniversitaet Leoben (Austria).

Bulk parameters: Sulphur (S), total inorganic carbon (TIC), and total organic carbon (TOC) contents are useful indicators of peat facies (e.g., Dai et al., 2020). Rock-Eval parameters S2 (amount of hydrocarbons generated during pyrolysis, mgHC/g rock), hydrogen index (HI = S2×100/TOC; mgHC/gTOC), and T_{max} (°C) provide information on the type and maturity of the organic matter (Espitalie et al., 1977). An Eltra Helios C/S analyzer and a Vinci Rock-Eval 6 instrument were used to determine these parameters in duplicate.

Organic petrography: The maceral composition of coal samples allows inferences on peat facies and diagenetic alterations. For maceral analysis, all samples were crushed to a maximum size of 1 mm and embedded in epoxy resin. The polished blocks were investigated using a Leica incident light microscope with a 50× oil-immersion objective, reflected white and fluorescent light, and a single-scan approach (Taylor et al., 1998). A total of 500 points were counted on each sample, with macerals assigned according to the ICCP system (ICCP, 1998, 2001; Pickel et al., 2017). Random huminite reflectance (%Rr) was measured to determine the coal rank of three samples. The measurements were performed in non-polarized light at a wavelength of 546 nm and a magnification of 50× using the Hilgers Fossil software. Mean values and standard deviation are based on 150 measurement points per sample.

Organic geochemical (biomarker) analyses were performed on eight coal samples to obtain information on the peat-forming vegetation. Samples were extracted with dichloromethane for 1 h at 75 °C and 100 bar in a Dionex ASE 350 extractor. After evaporation of the solvent to a total volume of 0.5 ml in a Zymark TurboVap 500 closed-cell concentrator, asphaltenes were precipitated from a hexane-dichloromethane solution (80:1) and separated by centrifugation. The hexane–soluble fractions were separated into aliphatic hydrocarbons, aromatic hydrocarbons and NSO compounds using a Köhnen-Willsch medium-pressure liquid chromatography (MPLC) instrument (Radke et al., 1980). *n*-Alkanes and isoprenoids in the aliphatic fractions were analyzed using a Trace GC-Ultra gas chromatograph with flame ionization detector (GC-FID). The gas chromatograph was equipped with a 50 m HP-PONA capillary column (0.20-mm inner diameter [i.d.], 0.50 µm film thickness). After sample injection (2 µl at 270 °C), the oven temperature was increased from 70 to 310 °C and kept constant for 35 min. The hydrocarbon fractions were analyzed using a gas chromatograph equipped with a 60 m TG-5MS fused silica capillary column (0.20 mm inner diameter; 0.25 µm film thickness) connected to a ThermoFisher ISQ mass spectrometer (GC-MS). The oven temperature was programmed from 40 to 310 °C at 4 °C/min, followed by an isothermal phase of 30 min. Helium was used as the carrier gas. The sample was injected in split mode (split ratio 20) at an injector temperature of 260 °C. The spectrometer was operated in EI (electron ionization) mode over a scan range from *m/z* 50 to *m/z* 650 (0.7 s total scan time). The Xcalibur software was used for data processing. Individual compounds were identified based on retention time in the total ion current chromatogram (TIC) and by comparing mass spectra to published reference data. The relative percentages and absolute concentrations of the various compound groups in the aliphatic and aromatic hydrocarbon fractions were calculated from the peak areas in the TIC chromatograms relative to the internal standards (squalane and 1,1'-binaphthyl, respectively) or by integrating the peak areas in the corresponding mass chromatograms using reaction factors to correct for the intensities of the fragment ion used to quantify total ion abundance. Concentrations were normalized to TOC.

Bulk carbon isotope data were determined on twelve coal samples. Portions of each sample (0.4 to 0.7 mg) were packed in tin capsules and burned in excess oxygen at 1080 °C using an elemental analyzer (Thermo Scientific Flesh EA). The CO_2 produced was analyzed online using a Thermo Scientific Delta-V isotopic ratio mass spectrom-

Sample	Lithology	Position (m above base)	Ash	Moisture	TOC	Sulphur	T_{max} (°C)	HI (mgHC/gTOC)	$\delta^{13}C$ (‰)	EOM	NSO	Ali.HC	Arom.HC
			(wt.% adb)		(wt.% db)					(mg/gTOC)			
BL1-roof	mudstone	20.4	89.07	4.2	0.73	0.02	425	39					
BL1-2	coal	19.9	2.12	27.6	49.3	0.10	390	170	-27.86				
BL1-3	coal	18.9	1.85	28.3	52.7	0.09	371	218					
BL1-4	coal	17.9	2.13	23.7	54.9	0.08	375	413	-27.99	441.0	8.5	0.5	0.4
BL1-5	coal	16.9	2.11	26.2	56.4	0.10	370	202					
BL1-6	coal	15.9	1.94	24.4	55.3	0.09	372	310	-27.81	301.6	11.8	0.8	0.4
BL1-7	coal	14.9	3.17	24.6	54.1	0.14	372	234					
BL1-8	coal	13.9	2.68	23.2	52.3	0.12	371	255	-27.82	273.6	8.4	0.7	0.6
BL1-9	coal	12.9	2.08	24.8	54.0	0.11	370	272					
BL1-10	coal	11.9	2.90	26.1	51.3	0.11	374	184	-27.54	221.4	6.6	0.7	0.4
BL1-11	coal	10.9	2.81	25.3	51.1	0.11	378	154					
BL1-12	coal	9.9	2.91	29.0	48.5	0.11	371	229	-27.68	231.8	3.9	0.3	0.2
BL1-13	coal	8.9	3.20	27.6	49.3	0.08	374	184					
BL1-14	coal	7.9	2.18	25.5	52.6	0.09	376	189	-28.06				
BL1-15	coal	7.4	2.45	27.0	51.3	0.09	371	204					
BL1-16a	coal	6.4	2.14	27.0	51.2	0.10	376	164	-28.04	217.2	6.4	0.7	0.4
BL1-16b	coal	6.2	7.54	22.1	51.3	0.09	371	240					
BL1-17	coal	5.4	1.90	27.5	52.5	0.10	372	185	-28.22				
BL1-18a	coal	4.4	1.94	27.8	53.0	0.09	375	230					
BL1-18b	coal	4.2	2.26	14.6	62.4	0.07	373	539	-28.26	305.4	4.2	0.3	0.1
BL1-19a	coal	3.2	4.52	17.9	55.4	0.16	395	195					
BL1-19b	coal	2.2	3.82	18.0	55.6	0.15	395	190	-27.74	246.0	5.4	1.2	0.8
BL1-20	mudstone	1.2	92.56	3.0	2.27	0.01	412	196					
BL1-21	coal	1	8.77	30.7	45.2	0.14	399	228	-27.70				
BL1-floor	mudstone	0	91.55	6.1	2.13	0.01	419	209					

Table 1: Bulk Parameters of Miocene Pit Jumbang coal. TOC – total organic carbon, HI – hydrogen index, EOM – extractable organic matter, NSO – hetero–compounds, adb – air-dried basis, db – dry basis, Ali.HC – aliphatic hydrocarbons, Arom.HC – aromatic hydrocarbons.

eter. The $^{13}C/^{12}C$ isotope ratio of CO_2 from a sample was compared to a reference ratio calibrated against the PDB standard. The overall reproducibility of the analytical procedure is in the 0.1 to 0.2 range.

4. Results

4.1 Bulk parameters

The bulk parameters of the studied samples are listed in Table 1. Their vertical distribution is shown in Figure 5. The ash yield in the BL1 seam is very low (1.8–8.8 wt.% adb). Slightly higher values are restricted to 20 cm thin layers beneath the main seam (8.8 wt.%) and between 6.2 and 6.4 m (7.5 wt.%). Moisture contents range from 23 to 31 wt.%, with three samples from the lower part of the seam having significantly lower contents (≤18 wt.%). Since moisture contents of coals in boreholes are typically around 35 wt.%, it is likely that the moisture content was reduced by air-drying.

The TOC content of the coal samples averages 52.7 wt.%. The TOC values of mudstones near the base of the coal seam (~2.2 wt.%) and above the seam (0.73 wt.%) are low. Sulphur contents are very low in all coal samples (0.07–0.16 wt.%) and even lower in the mudstone samples (0.01–0.02 wt.%). Despite the low sulphur contents, some vertical trends are visible: relatively high sulphur contents are observed in the lowermost part of the seam (1.0–4.2 m; ~0.15 wt.%), while a steady upward increase in sulphur content is observed between 4.2 and 15.9 m (0.07–0.14 wt.%). Above 15.9 m, the sulphur content is constant (~0.09 wt.%).

The hydrogen index (HI) of coal samples averages 236 mgHC/gTOC (154–539 mgHC/gTOC). The highest HI values occur at 4.2–4.4 m (539 mgHC/gTOC) and 17.9–18.9 m (413 mgHC/gTOC). Mudstone samples near the base of the seam have HI values around 200 mgHC/gTOC, while the organic-poor sample from the roof has a lower HI (39 mgHC/gTOC). T_{max} values of non-coal layers are in the range of 412–425 °C, while T_{max} values of coal samples are very low (370–399 °C).

Stable carbon isotope ($\delta^{13}C$) ratios of organic carbon range from -28.26 ‰ to -27.54 ‰. While $\delta^{13}C$ values of samples with HI <190 mgHC/gTOC cover the entire range of values, $\delta^{13}C$ values of samples with HI ≥190 mgHC/gTOC show a strong negative correlation with HI (r^2=0.93).

4.2 Biomarkers

Biomarker analysis was performed on eight coal samples. The extractable organic matter (EOM) of these samples is dominated by asphaltenes and NSO compounds, while aliphatic and aromatic hydrocarbons are subordinate (Fig. 6; Tab. 1). Chromatograms of the hydrocarbon fractions from samples taken from the lower, middle and upper parts of the BL1 seam are shown in Figure 7.

In all samples, the distribution of *n*-alkanes is dominated by long-chain *n*–alkanes (*n*-$C_{25–33}$), with a prominent odd-even predominance (Fig. 7). The concentration of *n*-C31 is remarkably high in most samples (Fig. 7). To visualize the differences in the composition of the *n*-alkanes, various parameters were calculated (Tab. 2). In Figure 6, these parameters are plotted as a function of stratigraphic position.

The ratio between long- and short-chain *n*-alkanes (*n*-$C_{27+29+31}$/*n*-$C_{15+17+19}$) is referred to as the terrestrial/aquatic ratio (TAR; Bourbonniere and Meyers, 1996). It ranges from 15 to 23 in most samples but is strongly elevated (37) in the upper sample (17.9–18.9 m). The P–aqueous ratio (Paq) is the ratio between medium- and long-chain *n*-alkanes ((*n*-C_{23}+*n*-C_{25})/(*n*-C_{23}+*n*-C_{25}+*n*-C_{29}+n-C_{31})) (Ficken et al., 2000). It is considered an indicator of the relative contribution of submerged and/or floating macrophytes. Between 2.2 and 16.9 m, the ratio varies between 0.21 and 0.27 with an overall slight upward increasing trend, while in the sample at 17.9–18.9 m it is significantly lower (0.17). The carbon preference index (CPI; Bray and Evans, 1961) reflects the relative contributions of land plants, but also maturity (Peters and Moldowan, 1993). In the BL1 coals, the average CPI is 3.7. Similar to TAR, CPI values are uniform in the main part of the seam (3.3–3.8), but elevated (4.8) in the sample at 17.9–18.9 m. The average

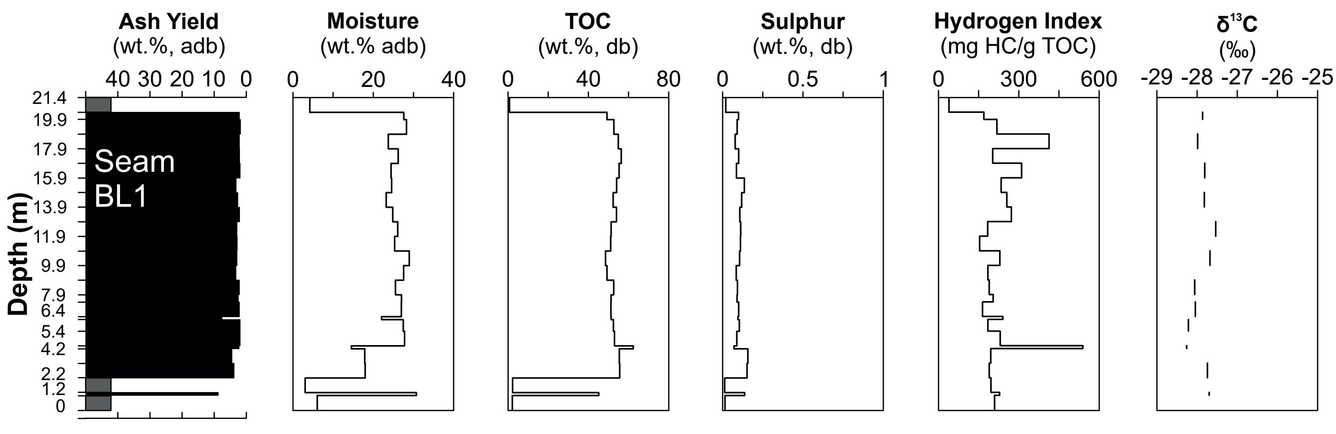

Figure 5: Vertical variation of bulk data: ash yield, moisture content, total organic carbon (TOC) content, sulphur content, hydrogen index, and stable carbon isotope ($\delta^{13}C$) ratios in seam BL1.

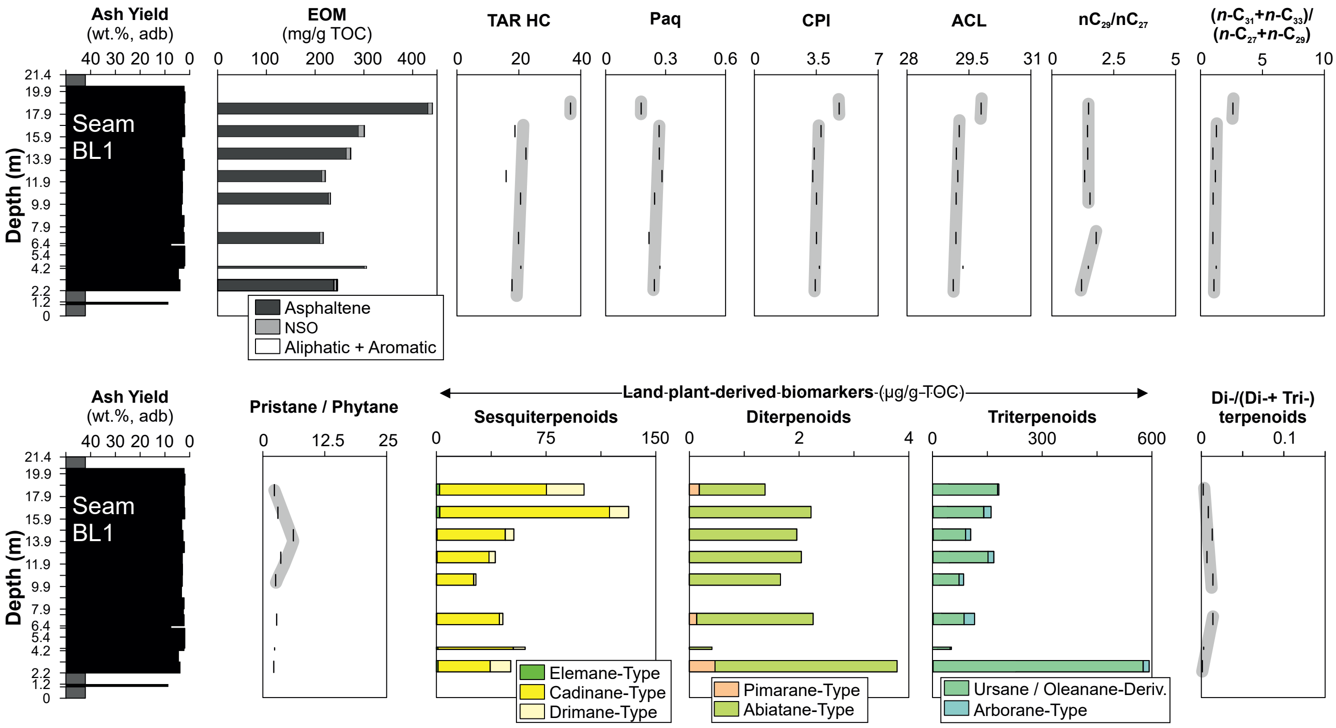

Figure 6: Variations of EOM, *n*-alkane and isoprenoid ratios and land plant–derived terpenoids in seam BL1. EOM = extractable organic matter; TAR HC = terrestrial/aquatic ratio (Bourbonniere and Meyers, 1996); Paq = P-aqueous (Ficken et al., 2000); CPI = carbon preference index (Bray and Evans, 1961); ACL = average chain length (Poynter and Eglinton, 1990).

chain length (ACL) of the long–chain *n*–alkanes was calculated according to Poynter and Eglinton (1990) (ACL = $(27n\text{-}C_{27}+29n\text{-}C_{29}+31n\text{-}C_{31})/(n\text{-}C_{27}+n\text{-}C_{29}+n\text{-}C_{31})$) to detect climatic changes. The values obtained range from 29.1 to 29.8 with the maximum value in the uppermost sample. The $n\text{-}C_{29}/n\text{-}C_{27}$ ratio (Buggle et al., 2010) and the $n\text{-}C_{31+33}/n\text{-}C_{27+29}$ ratio (Zech et al., 2009) can indicate changes in vegetation. The $n\text{-}C_{29}/n\text{-}C_{27}$ ratio increases from 1.2 to 1.8 in the lower part of the seam (2.2–7.4 m) and varies between 1.3 and 1.5 in the upper part. The $n\text{-}C_{31+33}/n\text{-}C_{27+29}$ ratio generally ranges between 1.0 and 1.3, but is significantly higher in the uppermost sample (2.6). The depth trends of ACL and of the $n\text{-}C_{31+33}/n\text{-}C_{27+29}$ ratio are almost identical (Fig. 6). The pristane/phytane (Pr/Ph) ratio is a widely used redox parameter (Didyk et al., 1978), but it is also strongly influenced by land plant input. The Pr/Ph ratio generally ranges from 2.2 to 3.6, but reaches a maximum (6.2) in the sample at 13.9–14.9 m depth.

Steranes occur in very low amounts and were not quantified, but land plant-derived tetra- and pentacyclic

Sample	TAR HC	Paq	CPI	ACL	nC_{29}/nC_{27}	nC_{31+33}/nC_{27+29}	Pr/Ph	Sesqui-	Di- terpenoids (µg/g TOC)	Tri-	Elem	Cadi	Drim	Pim	Abietane (µg/g TOC)	Lup	Olean - Urs	Ar-bor	Di-/(Di- + Tri-) terpenoids
BL1-4	36.7	0.17	4.8	29.8	1.5	2.6	2.3	101.0	1.4	181.3	1.9	64.2	22.6	0.1	0.8	0.5	43.9	3.5	0.008
BL1-6	18.7	0.26	3.8	29.3	1.4	1.3	3.1	131.5	2.2	160.3	1.9	97.1	11.0	0.0	1.8	1.6	38.9	19.8	0.014
BL1-8	22.3	0.26	3.4	29.2	1.5	1.0	6.2	53.0	2.0	104.4	0.4	39.7	5.0	0.0	1.8	2.0	23.8	13.9	0.018
BL1-10	15.9	0.27	3.3	29.2	1.3	1.2	3.6	40.3	2.0	167.7	0.4	30.4	3.7	0.0	1.9	1.5	45.6	15.9	0.012
BL1-12	20.5	0.24	3.5	29.2	1.5	1.0	2.6	27.0	1.7	85.0	0.1	21.8	1.3	0.0	1.5	1.0	17.2	12.4	0.019
BL1-16a	19.9	0.21	3.5	29.2	1.8	1.0	2.8	45.4	2.3	115.1	0.2	37.1	2.0	0.1	2.0	2.1	22.8	28.8	0.019
BL1-18b	20.6	0.26	3.7	29.4	1.5	1.3	2.4	60.7	0.4	51.7	1.0	47.1	7.4	0.0	0.3	0.2	12.3	3.6	0.008
BL1-19b	17.8	0.24	3.4	29.1	1.2	1.0	2.2	50.8	3.8	592.5	1.1	33.5	13.2	0.3	1.9	1.8	574.3	16.4	0.006

Table 2: Organic geochemistry of selected samples in seam BL1. TAR – terrestrial/aquatic ratio (Bourbonniere and Meyers, 1996); Paq – P-aqueous ratio (Ficken et al., 2000); CPI – carbon preference index (Bray and Evans, 1961); ACL – average chain length (Poynter and Eglinton, 1990); Pr/Ph – pristane/phytane ratio; Elem – elemane-type; Cadi – cadinane-type; Drim – drimane-type; Pim – pimarane-type; Abiet – abietane-type; Lup – lupane derivatives; Olean-Urs – oleanane-ursane derivatives; Arbor – arborane-type

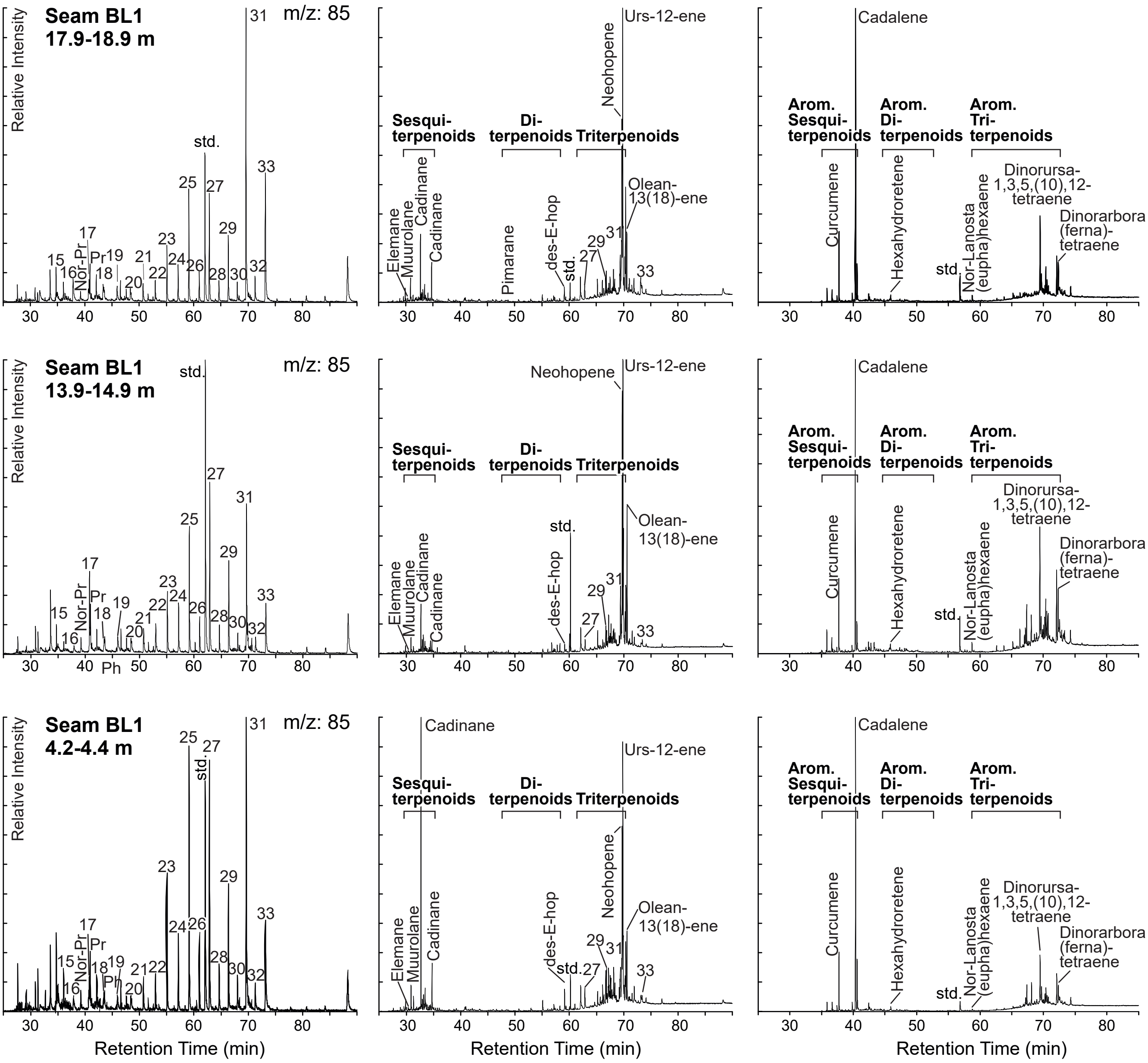

Figure 7: M/z 85 and total ion current (TIC) chromatograms of the aliphatic and aromatic hydrocarbon fractions of selected samples from seam BL1. The m/z 85 chromatogram shows the distribution of *n*-alkanes and isoprenoids. *N*-alkanes are labelled according to their carbon number; Pr = Pristane; Nor-Pr = Norpristane; Ph = Phytane; des-E-hop = des-E-hopane; Std = standard.

terpenoids are present in significant amounts (Tab. 2; Fig. 6). The dominant hopanoid compound is neohop-13(18)-ene (11.5–357.0 µg/gTOC). Aromatic hopanoids (D-ring monoaromatic hopane and benzohopanes) occur in minor amounts (0.16–2.09 µg/gTOC). Polyaromatic hydrocarbons (PAHs) were not detected. Saturated, unsaturated, and aromatic sesquiterpenoids of the cadinane (21.8–97.1 µg/gTOC) and drimane (1.3–22.6 µg/gTOC) types are observed in varying amounts (Fig. 7). The predominant cadinane types are muurolane, cadinane, cadinene, calamene, calamanene, tetrahydrocadalene, cadalene, and cadinatriene. Aliphatic drimane types are longifolene, eudesmane, and drimane. Elemane type sesquiterpenoids occur in small amounts (0.1–1.9 µg/gTOC).

Gymnosperm-derived diterpenoids occur in very low concentrations (Tab. 2). The occurrence of pimarane is limited to the lower part of the seam (≤0.3 µg/gTOC) and the uppermost sample (0.1 µg/gTOC). Abietane type diterpenoids (norabiete-triene and norabiete-tetraene) are present in all samples, albeit at very low concentrations (0.3–2.0 µg/gTOC). Angiosperm-derived triterpenoids are much more abundant than diterpenoids (Tab. 2; Fig. 7). They are dominated by ursane (urs-12-ene, dinorursa- 1,3,5(10),12-tetraene, tetramethyl-octahydropicene, dinor-oleana(ursa)-triene) and oleanane types (olean-12(18)-ene, olean-13(18)-ene, monoaromatic 8,14-seco-oleanane, dinoroleana-tetraene) (47.9–574.3 µg/gTOC). Arborane type (aromatic des-A-arbora-triene, norarbora(ferna)-triene, arbora(ferna)triene, dinorarbora(ferna)tetraene, dinoarbora(ferna)pentaene; 3.53–28.79 µg/gTOC) and lupane-derived (aromatic dinorlupatriene; 0.16–2.09 µg/gTOC) triterpenoids are less abundant. The di-/(di- + triterpenoids) ratio, a measure of the proportion of conifers versus angiosperms (Bechtel et al., 2003b), is very low (<0.02). Ratios >0.01 are restricted to the middle part of the seam (Fig. 6).

4.3 Maceral composition and huminite reflectance

Maceral percentages are listed in Table 3 and are plotted as a function of depth in Figure 8. Photomicrographs of typical macerals are shown in Figures 9 and 10. Huminite, derived from lignin and cellulose, is the predominant maceral group in most samples (47–75 vol.%). Huminite percentages (63–75 vol.%) are relatively high in the lower part of the BL1 seam (2.2–4.2 m), but decrease sharply (47 vol.%) in the thin layer between 4.2 to 4.4 m depth, which is characterized by the HI maximum. Above this level, the huminite content increases again and a reaches another maximum between 6.4 and 7.4 m (72 vol.%). The interval between 7.4 and 15.9 m is characterized by a general upward decrease in huminite to 47 vol.%. In the upper part of the seam (15.9–20.4 m), huminite percentages vary considerably, but display a general upward increase.

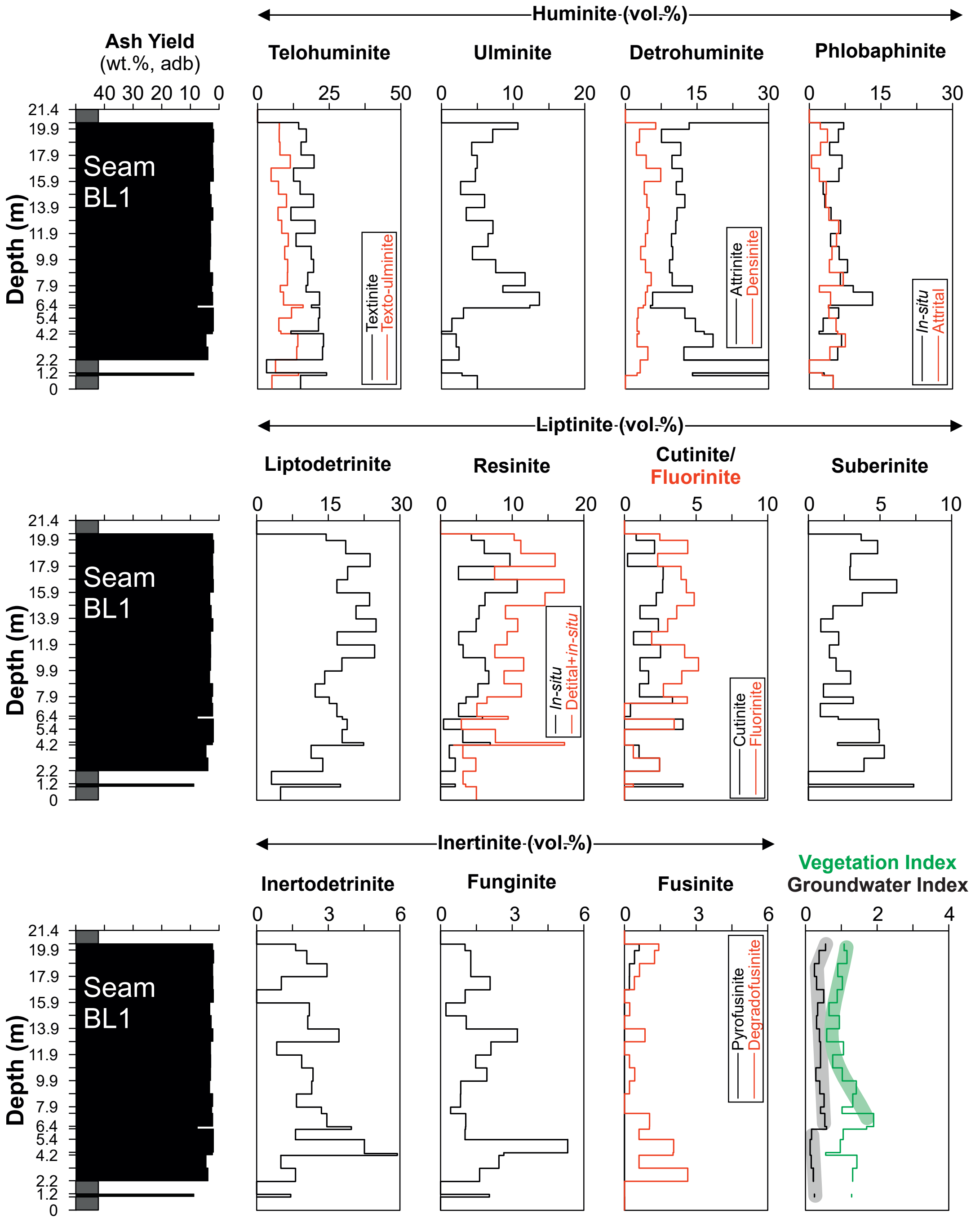

Figure 8: Variations of maceral percentages and petrography-based facies indicators in seam BL1.

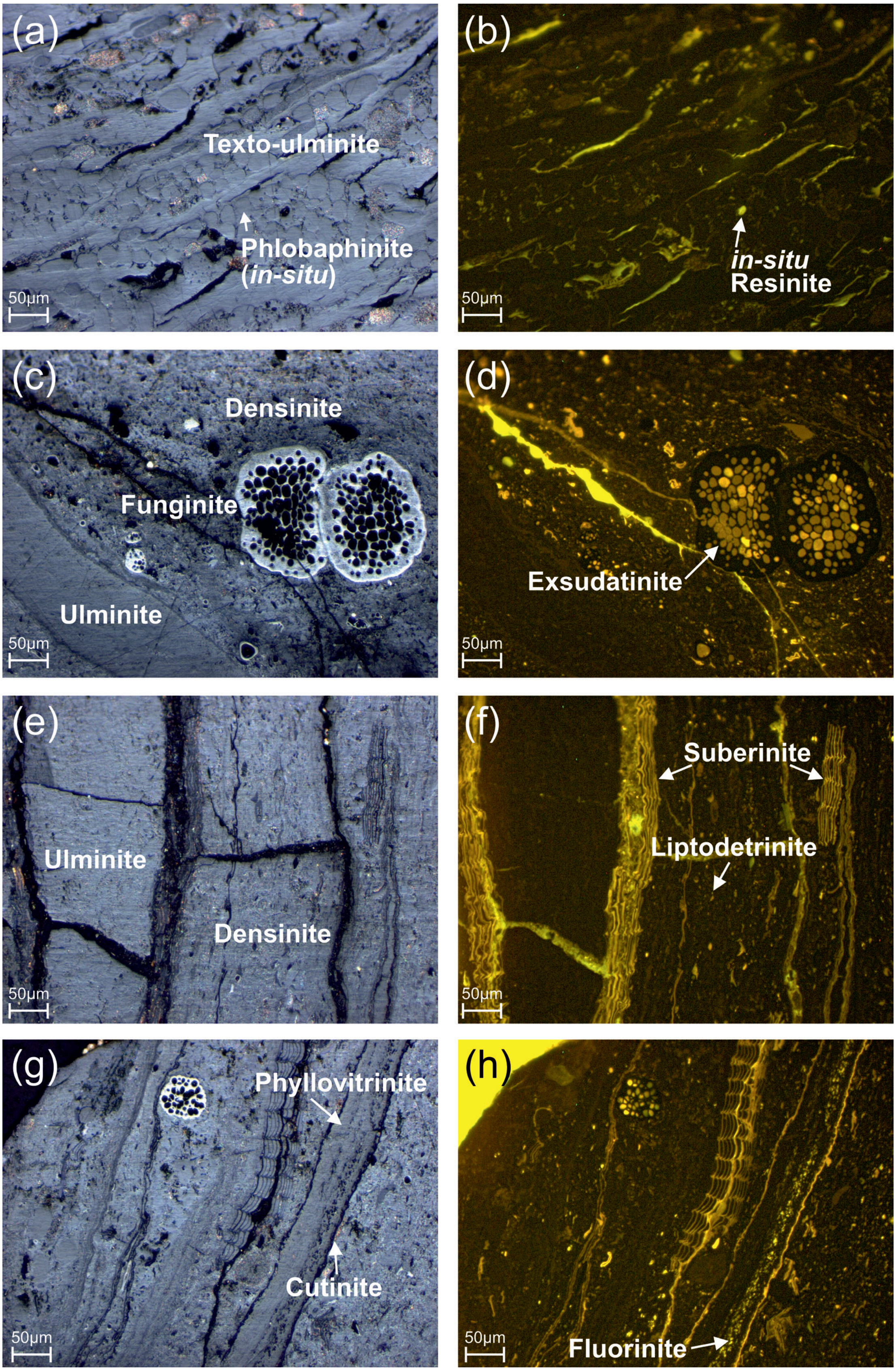

Figure 9: Representative photomicrographs of sample BL1 (3.2–4.2 m). Left: white light, right: blue light. **(a, b)** Texto-ulminite with *in-situ* phlobaphinite and resinite. **(c, d)** Ulminite and densinite with large funginite particles. Exsudatinite fills cavities inside of funginite. **(e, f)** Ulminite and densinite separated by suberinite. Liptodetrinite occurs together with humodetrinite. **(g, h)** Leaf with phyllohuminite, fluorinite, and cutinite in detrital coal with suberinite and funginite.

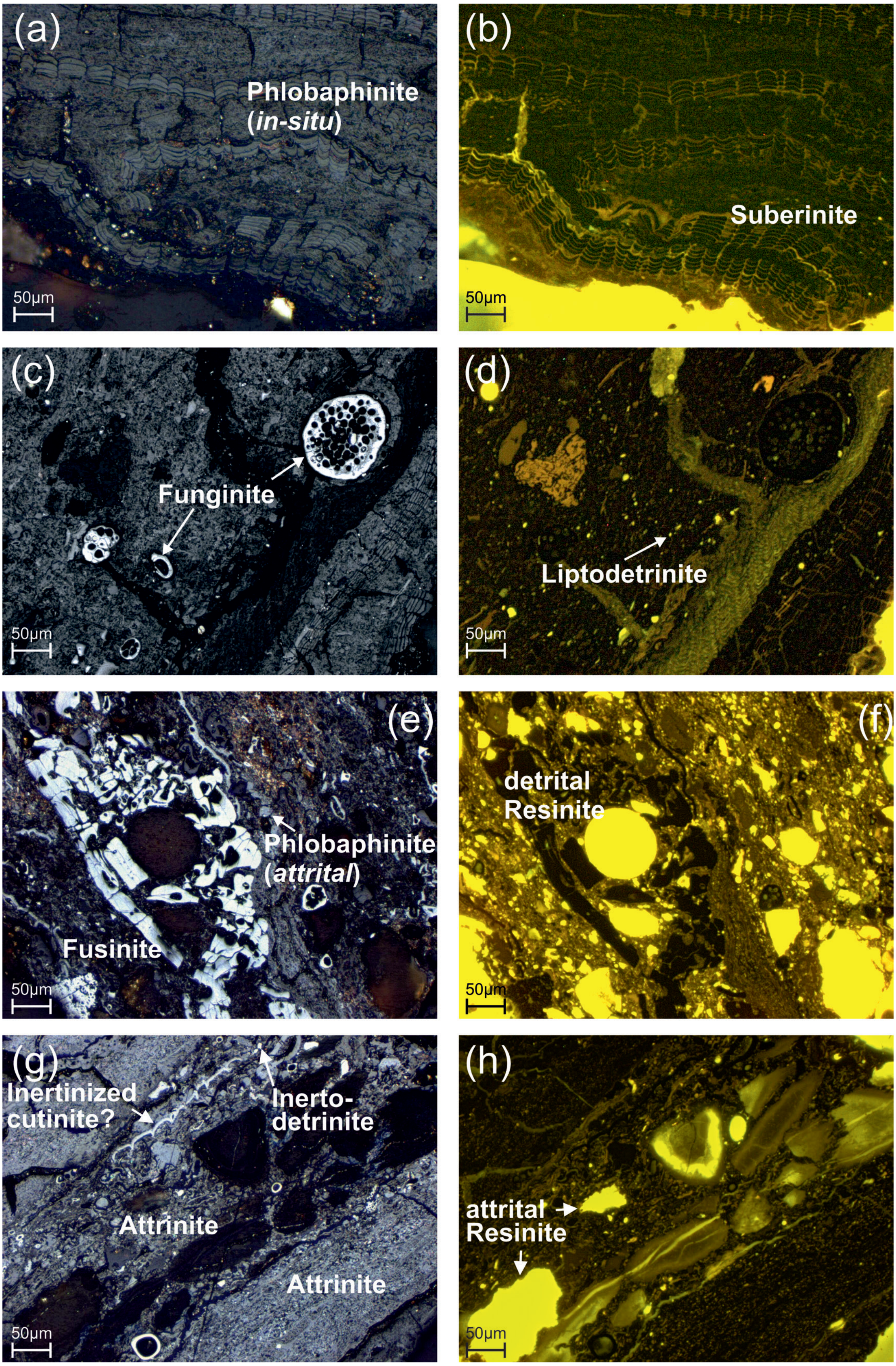

Figure 10: Representative photomicrographs of various samples from seam BL1. Left: white light, right: blue light. **(a, b)** 19.9–20.4 m; Coal rich in suberinite. Phlobaphinite occurs between suberinite. **(c, d)** 18.9–19.9 m; Attrinite matrix with funginite showing different sizes and shapes. **(e, f)** 4.2–4.4 m; Coal with high amounts of detrital resinite, fusinite and attrital phlobaphinite. The HI of this sample is exceptionally high (539 mgHC/gTOC). **(g, h)** 4.2–4.4 m; Attrinite and detrital resinite with inertodetrinite fragments. Inertinized cutinite(?) may be related to pathogenic fungi (cf. Arya et al., 2021; Fikri et al., 2022a). Alternatively, the oxidized structure may be interpreted as altered epidermal layers of roots (Moore et al., 1996).

Telohuminite (Fig. 9a-f) is the dominant huminite maceral. Detrohuminite (Fig. 9c-f) and gelohuminite occur in lower amounts. Phyllohuminite was recognized, but not counted separately (Fig. 9g). Phlobaphinite (cell fillings) is present both *in-situ* (in telohuminite; Fig. 9a) and attrital (Fig. 10e). Ungelified macerals (textinite, attrinite; Fig. 10g) are more abundant than gelified macerals (e.g., ulminite, densinite; Fig. 9c, e). Random huminite reflectance of three samples ranges from 0.33 to 0.35 %Rr (Table 3).

Liptinite, derived from hydrogen-rich plant components (e.g., resins, cuticules, etc.), occurs in significant amounts (21–50 vol.%) and shows an opposite depth trend compared to huminite. Thus, liptinite is most abundant in the thin layer between 4.2 to 4.4 m depth (42 vol.%) and in the layer between 14.9 and 15.9 m (49 vol.%), where the amount of liptinite is even higher than that of huminite. Liptinite is dominated by liptodetrinite (Figs 8, 9f, 10d; 11–25 vol.%). Resinite (fossil resins; Figs 9, 10) is also abundant (3–22 vol.%) and shows the same depth trend as the sum of liptinite macerals. It occurs *in–situ* (within telohuminite; Fig. 9a–b), detrital (Fig. 10e–h), and as the resinite variety fluorinite (leaf resins) (Fig. 9h). Detrital and *in–situ* resinite occur in similar amounts (Fig. 8). Resinite (*in–situ* + detrital) shows weak positive correlation with HI (r^2=0.48). Cutinite (Fig. 9g–h) occurs in varying proportions (max. 4 vol.%; Fig. 8), but its content is low in the coal layer beneath the BL1 seam and in its lower part. Sporinite occurs only in traces (max. 0.2 vol.%). Suberinite (fossil cork) (Figs 9g–h, 10a–b) is present in all samples in considerable amounts (0.8–7.3 vol.%).

Macerals of the inertinite group are less abundant (often 2–7 vol.%). Higher proportions (10–14 vol.%) are restricted to two intervals (4.2–5.4 m; 12.9–13.9 m). Inertodetrinite (Fig. 10g; up to 5.9 vol.%) and funginite (Figs 9c, g, 10c; up to 5.4 vol.%) are the dominant inertinite macerals. Pyrofusinite (Fig. 10e) occurs in notable amounts only in the uppermost seam (16.9–20.4 m; 0.2–0.6 vol.%). Degradofusinite is more abundant (up to 2.7 wt.%). Similar to pyrofusinite, its proportion increases in the uppermost part of the seam (up to 1.4 vol.%), but it is also present near the base of the seam (2.7 vol.%; Fig. 8).

5. Discussion

5.1 Maturity

Huminite reflectance (0.33–0.35 %Rr) and T_{max} values (<400 °C in coal samples, avg. 418 °C in non-coal layers) show the low maturity of the BL1 seam. This is supported by the high moisture content (~35 wt.% as received) and low calorific value of the coal, which classify the coal as lignite. Comparison with Miocene coal from the Tutupan mine in the Barito Basin, indicates that the Tutupan coal (0.36–0.41 %Rr; moisture: 18.8–26.3 wt.% in different seams) is slightly more mature.

5.2 Rheotrophic versus ombrotrophic and freshwater versus brackish peat formation

Rheotrophic (low-lying) and ombrotrophic (domed) mires are widespread in Southeast Asia. Peat accumulation in rheotrophic and ombrotrophic mires has also been proposed for Eocene and Miocene coals in south Kalimantan (e.g., Demchuk and Moore, 1993; Morley, 2013; Fikri et al., 2022a, b). Different mire-types can be distinguished based on basic parameters such as ash yield and sulphur content (e.g., Gruber and Sachsenhofer, 2001). These parameters are used in this section. In following sections, peat types are characterized in more detail based on biomarker and petrographic evidence.

Ash yields in the studied section range from 1.9 to 8.8 wt.%, with ash yields above 5 wt.% limited to the coal layer beneath the main seam (1.0–2.0 m) and a thin layer at 6.2–6.4 m (Fig. 5). Sulphur contents are also very low (0.08–0.16 wt.%). The borehole panel shown in Figure 4 indicates that low ash yield and low sulphur content are characteristic of the BL1 seam throughout the Jumbang mine. Low ash yields and low sulphur contents suggest deposition in a rainwater-fed ombrotrophic mire.

Slightly increased ash yields near the base of the seam could indicate a transition from an initial rheotrophic to an ombrotrophic setting. In the early stages of ombrotrophic mires, when roots were still reaching the nutrient-rich substrate, a slight increase in ash yield may also be due to uptake of inorganic substances. In some boreholes (5–6, 8–11, 16) not only ash yields, but also sulphur contents are increased in the lowermost part of seam BL1U. In several boreholes (e.g., 3, 11, 16 in Fig. 4), but not in the study section (Fig. 5), ash yields are also increased near the top of the seam. This may indicate a flooding event that finally terminated peat accumulation. Interestingly, this flooding is hardly reflected in the sulphur contents, which remain very low even in the uppermost samples (Fig. 4).

While sulphur contents in the BL1 seam are typically very low (<<0.5 wt.%), locally strongly elevated sulphur contents (1.0–1.5 wt.%) occur near the top of the lower coal bench (BL1L). This sharp increase in sulphur content is most evident in the lower coal bench in boreholes 5 to 8, which are located approximately 1 km southwest of the study section (Fig. 4). The high sulphur content in this area is a strong argument for the deposition of BL1L in a rheotrophic low-lying mire. Here, sulphur content is controlled by sulfate availability and the presence of sulfate-reducing bacteria, which is mainly controlled by acidity (e.g., Casagrande, 1987). The observed sulphur levels are consistent with deposition in a freshwater rheotrophic mire, where high water levels resulted in dilution of humic acids and an increase in pH. However, given the low ash yield of the sulphur-rich coals (Fig. 4) and the coastal depositional environment of the host rocks (e.g., Achmad, 2018), the high sulphur contents are most likely due to the influence of brackish water, underscoring the near-shore environment of the BL1 seam in the Jumbang mine.

It should be added that sulphur contents greater than 0.4 wt.% were not detected in Tutupan coals deposited in ombrotrophic or rheotrophic environments (Fikri et al., 2022a). This is likely due to their greater distance from the paleo-shoreline. In fact, Fikri et al. (2022a) postulated the formation of Tutupan seams T110 and T210 in kerapah (inland or watershed) swamps.

5.3 Nature of the peat-forming vegetation as recorded by geochemical data

The dominance of terrigenous plants in the coal organic matter is reflected in the distribution of *n*-alkanes and isoprenoids (Fig. 6). The *n*-alkane based parameters TAR (~19), Paq (~0.25) and CPI (~3.5) are quite uniform in the main part of the BL1 seam (2.2–16.9 m) showing the expected dominant role of land plants (Bourbonniere and Meyers, 1996; Ficken et al., 2000). An even stronger dominance of land plant is indicated by the biomarker data from the uppermost sample (17.9–18.9 m; Fig. 6). The dominant role of land plants is also confirmed by the Pr/Ph ratios (~3.2; e.g., Brooks et al., 1969; Powell and McKirdy, 1973), with the highest ratios are found in the middle part of the seam (13.9–14.9 m). A notable feature of the BL1 coal is the high concentration of *n*-C_{31} alkanes (Fig. 7), which is responsible for very high *n*-C_{31+33}/*n*-C_{27+29} ratios (average 1.3; Fig. 6). Following Schwark et al. (2002) and Zech et al. (2009), the dominance of *n*-C_{31} is attributed to the input of grasses and herbs.

Very low di-/(di- + triterpenoids) ratios (<0.02; Fig. 6) indicate that gymnosperms were rare in the peat-forming vegetation (cf. Bechtel et al., 2003b). Still low, but higher values were detected for Miocene coal in the Tutupan mine (0.01–0.12). Morley (2013) suggested that diterpenoid biomarkers in tropical peats from Southeast Asia may be derived from *Dacrydium* (Podocarpaceae) and possibly *Agathis* (Araucariaceae). He also noted that the presence of *Dacrydium* (together with the angiosperm Gymnostoma) is an indicator of kerapah swamps located at a greater distance from the paleo-shore line than basinal (or coastal) domed peats. Based on this information, Fikri et al. (2022a) postulated the deposition of Tutupan coal in kerapah swamps. In contrast to kerapah swamps, gymnosperms are largely absent from basinal mires (Morley, 2013). Therefore, the observed very low di-/(di- + triterpenoids) ratios in the BL1 coals support the deposition in a basinal peat growing behind mangrove swamps. This interpretation is further supported by the postulated near-shore environment. Low di-/(di- + triterpenoids) ratios (0.01–0.07) were also detected in middle and upper Miocene coals from the Kutai Basin by Widodo et al. (2009). These authors found a positive relation between $\delta^{13}C$ values (-28 to -27 ‰) and the di-/(di- + triterpenoids) ratios. Thus, the range of $\delta^{13}C$ values determined for the BL1 coals (-28.3 to -27.5 ‰), reflects the largely missing contribution of gymnosperms.

Among terpenoids derived from land plants, sesquiterpenoids of the cadinane type and triterpenoids of the ursane/oleanane type predominate. Cadinanes in present-day peats and Miocene coals in Southeast Asia are related to dammar resin produced by the angiosperm family *Dipterocarpaceae*, particularly the genus *Shorea* (e.g., Anderson, 1963; 1964; Anderson and Muller, 1975; Esterle and Ferm, 1994; Esterle et al., 1989; Cameron et al., 1989; Page et al., 1999; Wüst et al., 2001; van Aarssen et al., 1990, 1994; Widodo et al., 2009; Morley, 2013). A positive correlation between cadinane type sesquiterpenoids and the amount of *in-situ* resinite (r^2=0.63) provides additional support for the presence of dammar resin in the BL1 seam. The vertical distribution of the cadinane type sesquiterpenoids shows an upward increase in the upper part of the seam (~9–17 m) with a maximum (98 µg/gTOC) at 15.9–16.9 m (Fig. 6). Sequiterpenoids of the elemane type occur in small amounts. They may originate from gymnosperms (Otto and Wilde, 2001) or Magnoliaceae (Ding et al., 2019). Since their concentration shows a negative correlation with the di-/(di- + triterpenoids) ratio, a relation to Magnoliaceae is considered likely.

The concentration of arborane/fernane type triterpenoids is low. Arborane/fernane type triterpenoids are attributed to ferns or bacteria (e.g., Hauke et al., 1992). A fern source is considered likely because ferns are ubiquitous components of tropical vegetation in Southeast Asia (Demchuk and Moore, 1993; Morley, 2013).

Based on the near-shore environment and the virtual absence of gymnosperm biomarkers, the BL1 seam is presumed to have been deposited in a basinal peat swamp. Basinal peat swamps were studied in detail by Anderson (1963; 1964), who distinguished six phasic communities depending on decreasing soil fertility and increasing waterlogging. Phase 1 shows similarities with lowland rain forests, phase 2 shows less diversity with abundant *Shorea albida*, while phase 3 consists almost entirely of very large specimens of *Shorea albida*. Phase 4 and 5 lack emergent size trees and phase 5 lacks *Shorea albida*. Phase 6 represents open woodland or savanna where herbs are common (see also Morley, 2013). Given the above biomarker results, it is tempting to relate the maximum in cadinane type sesquiterpenoids (derived from dammar resin) at 15.9–16.9 m with phase 3 or 4 and the highest *n*-C_{31+33}/*n*-C_{27+29} ratio (indicating herbaceous vegetation) at 17.9–18.9 m to phase 6. Of course, palynological data are needed to support or refute this interpretation.

5.4 Petrography and mire types

The biomass of the original peat can be inferred from the abundance of specific macerals and of maceral ratios (e.g., Dai et al., 2020). The sum of the leaf-related macerals cutinite and fluorinite varies strongly from 0.0 to 7.7 vol.% (average 4.3 vol.%), but only samples from the lower part of the seam contain less than 0.1 vol.%. The percentages of cutinite and fluorinite are positively correlated in the lower part of the seam (2.2–7.9 m: r^2=0.92) and in the upper part (10.9–20.4 m: r^2=0.63) (Fig. 11), but the ratio

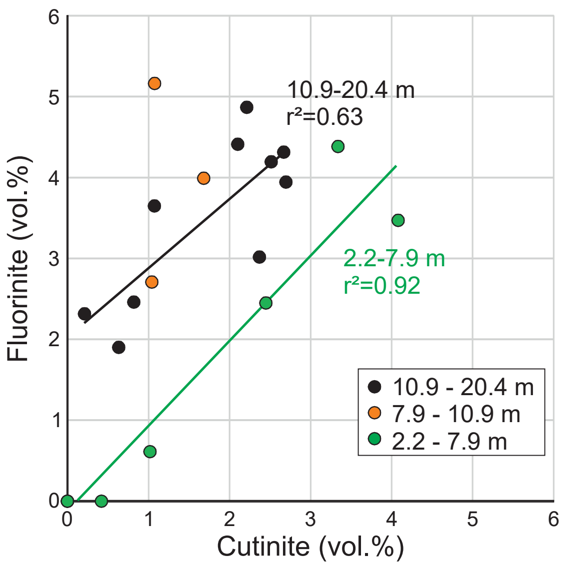

Figure 11: Plot of fluorinite versus cutinite percentages. Positive correlations exist for both samples from the lower part of the seam (2.2–7.9 m; r^2=0.92) and samples from the upper part (10.9–20.4 m; r^2=0.63), but the ratio of fluorinite to cutinite is higher in the upper part.

between fluorinite and cutinite is much higher in the upper part of the seam (7.9–20.4 m; Fig. 8). This indicates a change in leaf-forming vegetation at 7.9 m depth. It may be a coincidence, but some biomarker trends (e.g., Paq, n-C_{29}/n-C_{27}) show a break at roughly the same depth (cf. Fig. 6).

Suberinite is mainly derived from rootlets and occurs in high proportions in rheotrophic and ombrotrophic tropical mires (Fikri et al., 2022a, b). Suberinite contents are also very high in the Jumbang mine (0.9–7.3 vol.%; average 3.2 vol.%), especially in the lower and upper part of the BL1 seam (Fig. 8). Resins, both *in-situ* (4.6 vol.%) and detrital (4.7 vol.%), occur in high amounts in the BL1 seam. Their content increases upward in the seam, but the maximum percentage (17.7 vol.%) occurs in the thin layer between 4.2 and 4.4 m depth with very high HI (539 mgHC/gTOC). Resinite is also abundant in the clastic parting near the base of the seam. At least partly, resinite is derived from dammar resin (see section 5.3). In contrast to leaf- and root-derived macerals and resinite, sporinite is largely absent.

The proportion of inertinite macerals (excl. funginite) is low (1.2–8.6 vol.%; average 3.8 vol.%). This indicates that wildfires were very rare and that oxidation at the peat surface was limited. Small amounts of pyrofusinite in the uppermost part of the seam (Fig. 8) were probably wind-transported. Funginite is an inertinite maceral derived from fungal remains (0.2–5.4 vol%; average 1.6 vol.%). It occurs as unicellular spherical bodies and multicellular objects whose size can be well over 100 µm (Fig. 9c, d). Substantial amounts of funginite have been found in Miocene tropical coals (Demchuk and Moore, 1993; Fikri et al., 2022a) and in present-day ombrotrophic mires (Dehmer, 1993; Esterle and Ferm, 1994). Apparently, fungal activity played an important role in the decay and decomposition of dead plants (Adaskaveg et al., 1991; Hower et al., 2011a, b).

Various maceral-based facies indicators have been introduced to determine peat facies (e.g., Diessel, 1986; Calder et al., 1991; Markic and Sachsenhofer, 1997). Although poor agreement between petrographic, palynological, and geochemical data has been frequently reported (e.g., Wüst et al., 2001; Moore and Shearer, 2003; Dai et al., 2020; Fikri et al., 2022a), the use of these indicators is reasonable if all available non-maceral data and the fact that petrographic data reflect both changes in primary vegetation and degradation processes are taken into account (Demchuk and Moore, 1993; Wüst et al., 2001; Moore and Shearer, 2003; Fikri et al., 2022a,b). In the present paper, the vegetation index (VI) and groundwater index (GWI) of Calder et al. (1991) are applied. These parameters were developed for Pennsylvanian coal but appear to be applicable to coals of different ages, provided trends rather than absolute values are considered (Tab. 3; Fig. 8). VI is the ratio of preserved tissues to detrital macerals and is considered a proxy of the proportion of decay–resistant plants. GWI is the ratio of mineral matter plus gelified macerals to ungelified macerals and is considered an indicator of the wetness of the peat (Calder et al., 1991). VI and GWI are defined as:

VI = (humotelinite + phlobaphinite (*in-situ*) + fusinite + suberinite + resinite (*in-situ*)) / (detrovitrinite + phlobaphinite (attr.) + gelinite + inertodetrinite + sporinite + cutinite + liptodetrinite + fluorinite + resinite (detr.) + alginite)

GWI = (ulminite + densinite + collinite + mineral matter*) / (textinite + attrinite)
* Mineral matter (mm) has been calculated using the formula of Parr (1928) (mm = [1.08 x ash] + [0.55 x sulphur]).

The vegetation index (VI) is low (0.56–1.90; av. 1.10), reflecting moderate decomposition of the precursor plant material. The highest values (>1.7) are observed between 6.2 and 7.4 m. Above this level, VI decreases to 12.9 to 13.9 m, showing a slight increase only in the upper 7 m of the seam. The groundwater index (GWI) is very low (0.14–0.25) in the lower part of the seam (1.0–6.4 m) and low (0.25–0.59) in the upper part (6.4–20.4 m). Neither VI nor GWI can be correlated with geochemical parameters. Only GWI shows a weak positive correlation with the di- /(di- + triterpenoid) ratios (r^2=0.34), which might indicate that gymnosperms, if present, preferred moist conditions.

5.5 Comparison of Miocene ombrotrophic coals in Kalimantan and the Eastern Alps

Middle Miocene ombrotrophic coals are widespread in the Warukin Formation in Kalimantan, which formed during the post-rift/thermal sag stage of the Asem-Asem

Sample	Text.	Text-ulmi	Ulmi.	Attr.	Dens.	Pholabaphinite		Lipto-det.	Resinite		Cutin.	Fluor.	Suber.	Spor.	Pyro	Degra.	Fungi.	Inerto detr.	VI	GWI	%Rr.	Stdev
						in situ	detr.		*in situ*	detr.					Fusinite							
BL1-roof	0.0	0.0	0.0	100.0	0.0	0.0	0.0	0.0	0.0	0.0	0.0	0.0	0.0	0.0	0.0	0.0	0.0	0.0				
BL1-2	14.3	7.6	10.7	13.3	6.4	7.2	2.3	14.5	4.3	5.9	0.8	2.5	3.7	0.0	0.6	1.4	1.0	1.6	1.1	0.6		
BL1-3	17.0	7.6	7.1	7.6	2.9	6.1	3.8	18.7	6.1	5.0	2.1	4.4	4.8	0.0	0.4	1.3	1.3	2.1	1.2	0.4		
BL1-4	15.2	7.8	4.2	11.6	2.3	4.2	2.3	23.8	9.7	6.3	0.2	2.3	2.9	0.0	0.2	0.6	1.3	2.9	0.9	0.3		
BL1-5	19.7	11.4	5.0	9.8	4.4	6.8	0.4	19.1	2.5	5.0	2.7	3.9	2.9	0.0	0.2	0.4	2.1	1.0	1.0	0.3	0.35	0.02
BL1-6	12.5	4.7	4.7	11.9	7.4	6.2	2.1	16.8	10.7	6.6	2.7	4.3	6.2	0.0	0.0	0.0	1.0	0.0	0.9	0.5		
BL1-7	14.8	7.3	2.7	10.6	4.0	2.9	3.5	23.7	6.2	8.4	2.2	4.9	3.8	0.0	0.0	0.2	0.2	2.2	0.7	0.3		
BL1-8	19.5	10.1	6.0	12.4	4.5	3.2	3.4	20.8	5.4	3.6	1.1	3.6	1.7	0.0	0.0	0.0	1.1	2.1	0.9	0.3		
BL1-9	11.6	7.1	3.4	10.8	5.0	4.5	4.1	25.0	5.0	5.8	2.4	3.0	0.9	0.0	0.0	0.9	3.2	3.4	0.6	0.4		
BL1-10	20.0	8.4	7.2	10.5	4.6	6.5	6.1	16.9	2.5	6.8	0.6	1.9	2.1	0.0	0.0	0.0	2.1	0.8	1.1	0.4		
BL1-11	13.4	10.7	6.5	9.6	4.2	4.4	5.7	24.7	3.1	4.4	2.5	4.2	1.5	0.0	0.0	0.2	1.5	1.9	0.8	0.4	0.33	0.02
BL1-12	18.7	9.5	4.3	9.9	3.2	6.2	4.7	17.8	6.2	5.4	1.1	5.2	1.9	0.0	0.0	0.4	1.9	2.4	1.0	0.3		
BL1-13	19.5	10.5	7.6	9.2	4.2	8.0	4.2	14.3	6.7	2.1	1.7	4.0	2.9	0.0	0.0	0.2	0.8	2.3	1.4	0.4		
BL1-14	17.5	10.4	11.7	9.8	5.4	6.5	7.1	12.3	5.2	6.0	1.0	2.7	1.0	0.0	0.0	0.0	0.8	1.7	1.3	0.5		
BL1-15	16.9	7.9	8.6	14.0	4.6	9.2	2.1	15.2	3.5	2.9	3.3	4.4	3.1	0.0	0.0	0.0	0.4	2.7	1.0	0.4		
BL1-16a	21.6	9.0	13.7	5.7	4.2	13.2	4.4	16.8	2.5	2.5	0.4	0.0	0.8	0.0	0.0	1.1	1.1	2.9	1.9	0.5	0.35	0.02
BL1-16b	18.8	15.9	12.3	5.2	3.8	4.0	4.0	18.0	5.8	3.5	0.0	0.0	2.1	0.0	0.0	1.0	1.0	4.0	1.7	0.6		
BL1-17	21.6	11.8	3.1	12.4	2.7	6.1	4.1	19.0	0.4	2.4	4.1	3.5	4.9	0.0	0.0	0.6	1.0	1.6	1.1	0.2		
BL1-18a	21.2	7.4	1.4	14.6	2.5	2.9	5.6	17.9	3.1	4.5	0.0	0.0	4.9	0.0	0.0	2.1	5.4	4.5	1.0	0.1		
BL1-18b	11.6	8.1	0.0	16.5	2.9	2.0	5.9	22.4	6.9	10.4	0.0	0.0	2.0	0.0	0.0	2.0	2.6	5.9	0.6	0.1		
BL1-19a	23.0	14.1	2.0	18.3	2.4	6.7	7.5	11.4	1.2	1.8	1.0	0.6	5.3	0.0	0.0	0.6	2.4	1.0	1.4	0.2		
BL1-19b	22.7	13.7	2.4	12.2	4.7	5.9	4.3	13.9	2.0	2.9	2.4	2.4	3.9	0.2	0.0	2.7	1.6	1.6	1.3	0.2		
BL1-20	3.1	6.3	0.0	81.3	3.1	0.0	0.0	3.1	0.0	3.1	0.0	0.0	0.0	0.0	0.0	0.0	0.0	0.0				
BL1-21	24.1	14.3	2.9	14.1	2.4	3.1	2.7	17.6	2.0	1.4	4.1	0.6	7.3	0.0	0.0	0.0	2.0	1.4	1.3	0.3		
BL1-floor	15.0	5.0	5.0	55.0	0.0	5.0	5.0	5.0	0.0	5.0	0.0	0.0	0.0	0.0	0.0	0.0	0.0	0.0				

Table 3: Maceral percentages (in vol.%), maceral–based facies indicators (VI, GWI), and random huminite reflectance (%Rr). Text. – textinite, Ulmi. – ulminite, Attr. – attrinite, Dens. – densinite, Liptodet. – liptodetrinite, Cutin. – cutinite, Fluor. – fluorinite, Suber. – suberinite, Spor. – sporinite, Fungi. – funginite, Inertodetr. – inertodetrinite, VI – vegetation index, GWI – groundwater index. stdev – standard deviation.

and Barito basins (e.g., Friederich et al., 2016). Coals of the same age formed in warm-temperate to subtropical climate in small pull-apart basins in the Eastern Alps (Fig. 12a). The coal in the Leoben Basin was formed in an ombrotrophic setting (Gruber and Sachsenhofer, 2001). This allows comparison of ombrotrophic coals of the same age, but formed in different climates and basin types. Key parameters of these coals are summarized in Table 4 and shown in a cartoon-like illustration in Figure 13.

5.5.1 Climate and mire types

The tropical wet climate that prevailed in Kalimantan since Eocene time (Morley, 2012) favored middle Miocene coal accumulation in basinal and kerapah domed mires and in rheotrophic mires. Data published in this paper suggest that the Jumbang coal (seam BL1) was formed in a basinal mire (Fig. 13a). In contrast, coal exploited at the Tutupan mine was formed in kerapah mires (seams T110, T210; Fig. 13b) or in mixed rheotrophic/ombrotrophic mires (seam T300; Fikri et al., 2022a, b).

A warm, subtropical climate prevailed in the Eastern Alps during the (early) middle Miocene (e.g., Jiménez-Moreno et al., 2008). A rich flora has been described from the Leoben Basin (e.g., Ettingshausen, 1888) and the nearby Parschlug Basin (Kovar-Eder et al., 2022; see Fig. 12 for location). The Parschlug flora indicates a subtropical climate with pronounced seasonality (Csa, Csb according to Peel et al., 2007; Kovar-Eder et al., 2022). In contrast, a humid subtropical warm-temperate climate without distinct seasonality is indicated for the Leoben area (Cfa according to Peel et al., 2007; Kovar-Eder, pers. comm., 2023). We suspect that local climatic conditions in the Leoben area may have favoured the formation of an ombrotrophic mire (Fig. 13c), whereas ombrotrophic mires did not form in other areas in the Eastern Alps. Ash yield in the Leoben coal is very low and increased only in coal benches with diagenetic siderite concretions (Fig. 12b).

Peat accumulation rates may be influenced by climate. The average present-day peat accumulation rate of tropical peat in Southeast Asia is 1.3 mm/year (e.g.,

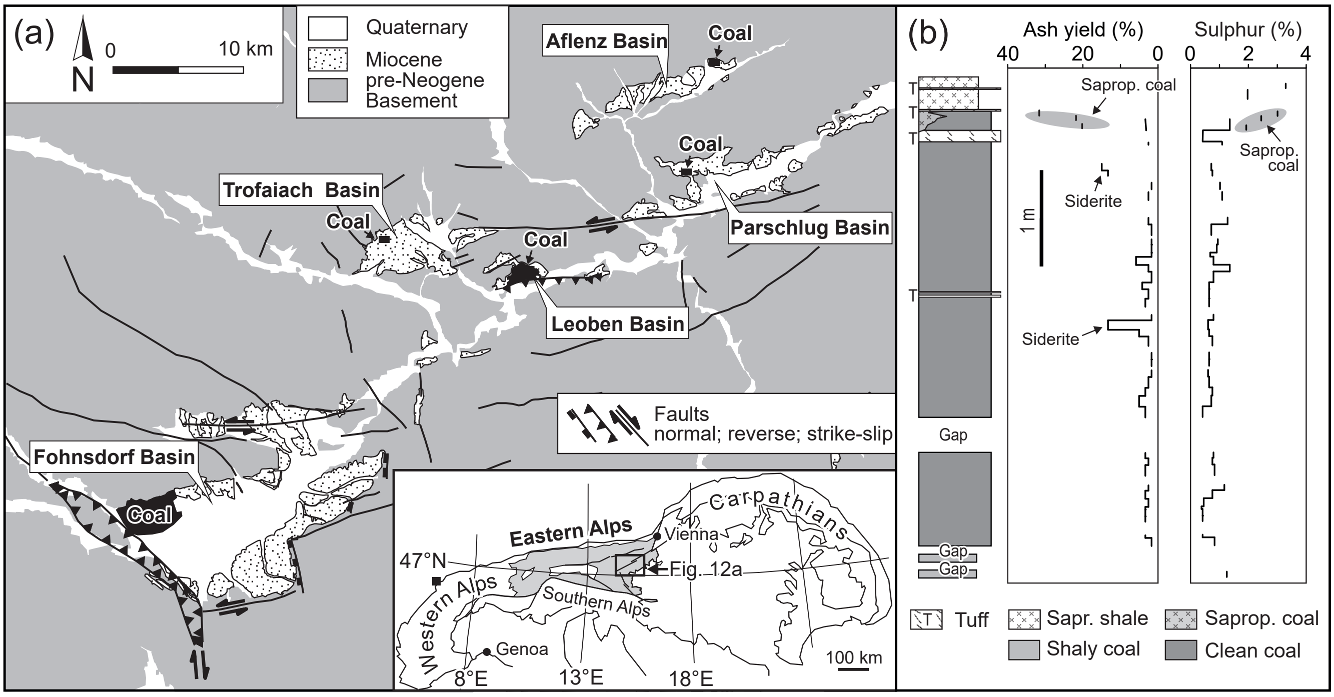

Figure 12: (a) Position of Miocene coal-bearing pull-apart in the Eastern Alps. Coal in the Fohnsdorf, Trofaiach, Aflenz and Parschlug basins was formed in low-lying mires, while coal in the Leoben Basin was formed in an ombrotropihc domed mire (Sachsenhofer et al., 2003). **(b)** Ash yields and sulphur contents of the coal seam in the Leoben Basin (after Gruber and Sachsenhofer, 2001).

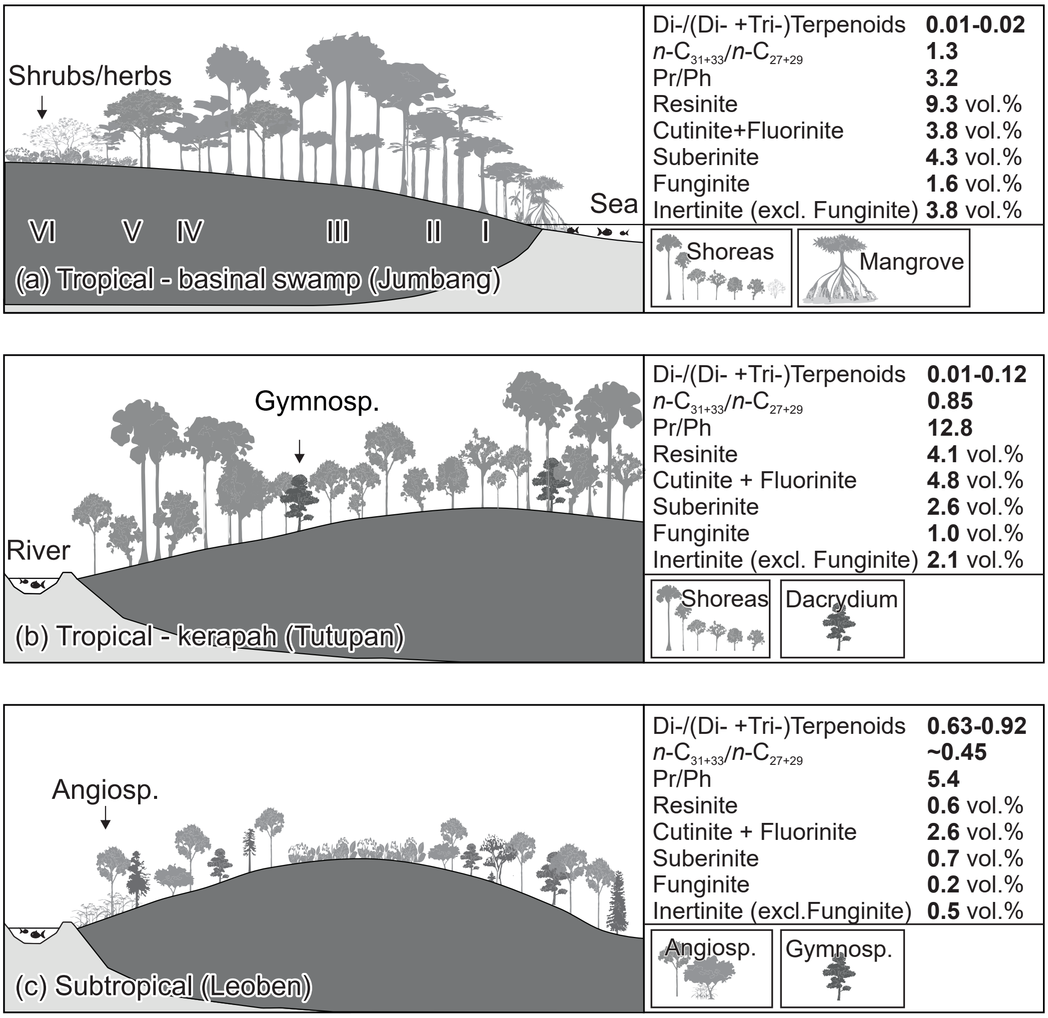

Figure 13: Cartoons showing middle Miocene peat forming environments in **(a)** tropical basinal swamp (Jumbang), **(b)** tropical kerapah swamp (Tutupan) and **(c)** in subtropical ombrotrophic mire (Leoben). Tropical vegetation in basinal swamp (phasic communities I-VI) according to Anderson (1963; 1964), Anderson and Muller (1975) and Morley (2003).

Page et al., 2010), with very few data exceeding 4.5 mm/year. However, average ombrotrophic peat accumulation rates in cool climates in northern Europe are in a similar range (0.5–3.5 mm/year; Stivrins et al., 2017), indicating that ombrotrophic peat growth rates are not necessarily higher in tropical areas.

5.5.2 Basin type, seam geometry and peat accumulation rates

Major differences exist between number, thickness, and lateral continuity of seams. The Miocene coal seams in Kalimantan formed during the post-rift/thermal sag stage of basin evolution (e.g., Friederich et al., 2016). During this basin stage, faulting is minor and subsidence often moderate, favouring the accumulation of multiple, laterally extensive coal seams. Three seams of exceptional thickness are present at the Tutupan mine (Fikri et al., 2022a) and many seams, although not all mined, are present in the Jumbang area (Fig. 2b). In contrast, coal in the Eastern Alps formed in late-orogenic pull-apart basins with limited lateral extent (Fig. 12a; Sachsenhofer et al., 2003). A single thick seam overlain by sapropelic coals and shales (Fig. 12b) is characteristic of this setting characterized by very high subsidence rates (Sachsenhofer, 2000).

The very large thickness of single Tutupan seams (up to 50 m) shows that subsidence rates were in equilibrium with peat accumulation for a long time. Geochemical data demonstrate that the large thickness of the Tutupan coals is the result of stacking of several coal cycles (Fikri et al., 2022a). No such stacking was observed in the Jumbang or Leoben coals. In case of coals in pull-apart basins, the high subsidence rates prevent the evolution of multiple cycles (cf., Markic and Sachsenhofer, 1997).

5.5.3 Sulphur contents and brackish/marine influence

All coals considered accumulated in freshwater mires. However, sulphur contents are locally elevated in the lower coal bench BL1L in the Jumbang mine (Fig. 4; section 5.2) suggesting deposition in a near-shore environment, possibly behind coastal mangroves (Fig. 13a). Coal layers with locally increased sulphur contents, therefore, may be used as marker for ombrotrophic basinal coals.

The average sulphur content in the Leoben coal is 0.65 wt.%. Relatively high sulphur contents in the lowermost ash-rich samples represent an early rheotrophic stage, whereas sulphur contents >1 wt.% in the uppermost 20 cm (Fig. 12b) may be related to volcanic activity rather than a brackish environment (Gruber and Sachsenhofer, 2001; Widodo et al., 2010).

5.5.4 Differences in vegetation between tropical and subtropical ombrotrophic mires as reflected by geochemical and petrographic data

Miocene vegetation in tropical ombrotrophic mires is dominated by angiosperms, but small amounts of gymnosperms are present in kerapah peat (e.g., Anderson and Muller, 1975; Morley, 2013; Fig. 13a, b). The peat-forming vegetation of the Leoben coal is unknown. Considering results from the ombrotrophic coal in the Lower Rhine Basin (e.g., Figueiral et al., 1999; Stock et al., 2016; LRB in Fig. 1a), angiosperm-dominated vegetation with substantial amounts of gymnosperms, rich in shrubs and mosses can be assumed (Fig. 13c). Differences in gymnosperm abundance are clearly reflected in the di-/(di- + triterpenoids) ratios, which are very low in basinal and tropical rheotrophic coal, low to moderately high in kerapah coals, and high in subtropical Leoben coals (Tab. 4, Fig. 13).

Other geochemical differences include significantly lower Pr/Ph and significantly higher n-C_{31+33}/n-C_{27+29} ratios in coals from basinal peats (Fig. 13a) compared to kerapah peat (Fig. 13b). Because of the lower maturity of the Jumbang coal, these differences are attributed to differences in primary vegetation rather than maturity. The Pr/Ph ratio in the Leoben coal occupies an intermediate position. The n-C_{31+33}/n-C_{27+29} ratio in the Leoben coal is not discussed, as it may be reduced by the slightly higher maturity of this coal. The same is applies to the CPI, which is significantly lower in Leoben coal than in other coals.

Dammar resin-producing *Dipterocarpaceae* (e.g., *Shorea*) are characteristic floristic elements in Miocene coals from Southeast Asia. A positive correlation between cadinane type biomarkers and total resinite content for 56 Miocene coals from Kalimantan (r^2=0.62) supports the relation between cadalene and dammar resin in the tropical coals. Therefore, the higher cadinane concentration and higher resinite percentage in the Jumbang coal compared to the Tutupan coal support a higher contribution of *Dipterocarpaceae* in basinal peats. Cadinane type biomarkers are also present in the Leoben coal. As dipterocarps are restricted to the tropical zone, cadinanes in Leoben coal must have a different source. Bechtel et al. (2001) linked cadinanes in the Leoben coal to members of the Coniferales families.

There are also large differences in the maceral composition between tropical and subtropical ombrotrophic coals (Tab. 4, Fig. 13). Resinite is significantly more abundant in tropical coals than in subtropical coals. This could be due to the absence of dammar resin-producing dipterocarps outside the tropical zone. Among tropical coals, the average resinite percentage is more than twice as high in basinal compared to kerapah coal. Rootlet-derived suberinite is an important constituent in all tropical coals, but is much less abundant in subtropical coal. Some layers in the subtropical Leoben coal are very rich in leaf-derived macerals (max. 21 vol.%), but on average the amount of leaf-derived macerals is higher in tropical coals.

Funginite is present in significant amounts in tropical coals from Kalimantan (average 1.0–1.6 vol.%) and in present–day tropical peats (e.g., Demchuk and Moore, 1993; Dehmer, 1993; Esterle and Ferm, 1994), but in low

	Jumbang Mine	Tutupan Mine		Leoben Mine
Peat–type	ombrotrophic (basinal)	ombrotrophic (kerapah)	ombrotrophic + rheotrophic	ombrotrophic
Rank	Lignite A	Subbituminous C		Subbituminous A
Climate (Friederich et al., 2016; Kovar-Eder, pers. comm., 2023)	Tropical ever–wet	Tropical ever–wet		Warm temperate (Cfa)
Number of economic seams	1 (-3)	3		1
Lateral continuity	high	high		Restricted
Seam names	BL1	T110, T210	T300	Leoben seam
Thickness of single seams	20 m	up to 50 m	24 m	up to 16 m
Stacked successions (cycles)	no	yes (up to 5)	unclear (2?)	no
Marine/brackish influence	Local brackish influence in BL1U	––	––	––
Vegetation (Morley, 2013)	Angiosperm trees (e.g., Shorea)	Angiosperm trees (e.g., Shorea) (+gymnosperms)		??
Gymnosperms (Di–/(di- +Tri-)Terpenoids)	Very rare (0.01-0.02)	Rare (0.01-0.12)	Very rare (0.01-0.04)	High (0.63-0.92)
CPI	3.7 (3.3–4.8)	4.3 (2.8–6.2)	3.1 (2.2–3.8)	1.4 (1.1-2.8)
TAR	21.6 (15.9-36.7)	10.4 (5.8–23.4)	19.9 (6.0–38.4)	~15
Paq	0.24 (0.17-0.27)	0.14 (0.05–0.24)	0.08 (0.05–0.11)	~0.6
ACL	29.3 (29.1-29.8)	29.1 (28.2–30.6)	29.5 (29.0–30.0)	~28.8
n–C_{29}/n–C_{27}	1.47 (1.20-1.80)	1.39 (0.77–2.33)	3.14 (2.09–4.83)	~1.2
n–C_{31+33}/n–C_{27+29}	1.3 (1.0-2.6)	0.85 (0.17–2.23)	0.67 (0.46–0.91)	~0.45
Pr/Ph	3.2 (2.2-6.2)	12.8 (5.4–23.6)	6.1 (3.9–8.1)	5.4 (2.0-7.1)
Degradation (Vegetation Index)	Moderate (1.10)	Low (1.56)	Low (1.26)	Moderate (1.0)
Water table (GWI) / extent of external influx	Low (0.35)	Low (0.17)	Low (0.32)	Low (~0.1)
Resins (*in–situ*+detrital; vol.%)	Very abundant 9.3 (2.9-17.3)	Abundant 4.1 (1.0–19.1)	Abundant 4.0 (0.8–9.0)	Rare 0.6 (0.0-2.7)
Cadinane–source	Dammar resin (dipterocarps)	Dammar resin (dipterocarps)	Dammar resin (dipterocarps)	Conifer resins
Leafs (cutinite+fluorinite; vol.%)	abundant 4.3 (0.0–7.7)	abundant 4.8 (0.4–13.1)	abundant 3.8 (0.6–8.5)	rare to abundant 2.6 (0-20.8)
Roots (suberinite; vol.%)	very abundant 3.2 (0.0-7.3)	abundant 2.6 (0.2–7.0)	abundant 2.0 (0.4–4.6)	rare to abundant 0.7 (0.0-5.8)
Alginite	––	––	traces	––
Fungal activity (funginite; vol.%)	high 1.6 (0.2–5.4)	high 1.0 (0.0–3.2)	high 1.5 (0.6–2.8)	Low 0.2 (0.0-1.2)
Inertinite (excl. funginite; vol.%)	3.8 (1.2-8.6)	2.1 (0.0–4.0)	2.3 (0.6–5.0)	0.5 (0.0-2.4)

Table 4: Summary of similarities and differences between middle Miocene ombrotrophic coals in Kalimantan and the Eastern Alps. Data from the Tutupan and Leoben mines are from Fikri et al. (2022a) and Gruber and Sachsenhofer (2001) and Bechtel et al. (2001), respectively.

amounts in subtropical Leoben coal (average: 0.2 vol.%). This indicates that Eh and pH conditions were less favourable to fungal activity in subtropical peatlands. The amount of oxidized plant material in tropical coals is low (average 2.1–3.8 vol.%), but even lower in the subtropical Leoben coal.

6. Conclusions

The purpose of studying the BL1 coal seam in the Jumbang mine (south Kalimantan) was threefold. First, to reconstruct the depositional environment of peat in the middle Miocene Asem-Asem Basin. Secondly, to compare the middle Miocene peat facies in the Asem-Asem and Barito basins based on coal data from the Tutupan mine. Finally, the tropical coals should be compared with the subtropical Leoben coal of the same age in the Eastern Alps.

Several middle Miocene coal seams are present in the Jumbang mine, but only the BL1 seam, up to 20 m thick, is mined. The lignite seam was investigated using a multi–method approach including analysis of ash yield, carbon and sulphur content, Rock–Eval pyrolysis, organic geochemistry, and petrology. The BL1 seam is locally underlain by a coal bench (BL1L) that has a high sulphur content. Together with the facies of the host rocks, this indicates a near-shore environment. In contrast to the lower coal bench, the main seam contains low-ash, low-sulphur coal that represents peat accumulation in an ombrotrophic mire. According to biomarker data, the vegetation was dominated by angiosperms, including a large number of dammar resin-producing dipterocarps. Biomarkers for gymnosperms are very rare, suggesting deposition in a basinal (coastal) domed mire.

Ash yields, sulphur contents and geochemical and petrographic parameters of the BL1 seam are similar to those of the tropical Tutupan T110 and T210 seams in the Barito Basin, which accumulated in a kerapah (or inland) swamp. However, the concentration of cadinane type biomarker and the percentage of resinite are significantly higher in the BL1 seam, which is probably related to the abundance of *Shorea albida* in the basinal mire.

The comparison of the tropical ombrotrophic coals (Jumbang, Tutupan) with the subtropical ombrotrophic Leoben coal shows that the latter contains a significantly higher amount of gymnosperm-derived biomarkers. Moreover, the percentage of resinite, leaf- and rootlet derived macerals is significantly lower in the subtropical coal. The low amount of resinite is at least partly due to the absence of dipterocarps. The low amounts of funginite show that fungal activity was reduced in the subtropical peat. In addition, the amount of oxidized plant tissues (inertinite without funginite) is much lower in the subtropical coal studied.

Overall, the comparison of the Jumbang, Tutupan, and Leoben coals shows minor differences between ombrotrophic coals from kerapah and basinal mires, but major differences between tropical coals from Kalimantan and the subtropical ombrotrophic Leoben coal. Further investigations and a larger database are needed to show whether these differences are site-specific or general.

Acknowledgments

The first author (FHN) thanks OeAD, Austria´s Agency for Education and Internationalization, for an Ernst Mach Grant, ASEA-UNINET scholarship (Reference number: ICM-2019-13766, MPC-2020-01500, MPC-2021-01331, MPC-2021-01480). FHN would also like to thank PT Jhonlin Baratama and PT Arutmin Indonesia for their help in sampling the coal seams. We thank Johanna Kovar-Eder for as yet unpublished paleoclimate data on the Leoben site. The paper benefited from constructive reviews by Sri Widodo (Hasanuddin University, Indonesia) and Ksenija Stojanovics (University of Belgrade).

References

Achmad, A., 2018. Key of Meratus Complex Uplift: Sedimentological approachment of Ophiolitic Fragments within Warukin Sandstones in Asem - Asem Basin. Proceedings Pekan Ilmiah Tahunan IAGI, 28th Oct-1st Nov, 2018.

Adaskaveg, J.E., Blanchette, R.A., Gilbertson, R.L., 1991. Decay of date palm wood by white-rot and brown rot fungi. Canadian Journal of Botany, 69/3, 615–629. https://doi.org/10.1139/b91-083

Advokaat, E. L., Marshall, N.T., Li, S., Spakman, W., Krijgsman, W., van Hinsbergen, D. J., 2018. Cenozoic rotation history of Borneo and Sundaland, SE Asia revealed by paleomagnetism, seismic tomography, and kinematic reconstruction. Tectonics, 37/8, 2486–2512. https://doi.org/10.1029/2018TC005010

Anderson, J.A.R., 1963. The flora of the peat swamp forests of Sarawak and Brunei, including a catalogue of all recorded species of flowering plants, ferns and fern allies. The Gardens´ Bulletin, Singapore, 20/2, 131–238.

Anderson, J.A.R., 1964. The structure and development of the peat swamps of Sarawak and Brunei. Journal of Tropical Geography, 18, 7–16.

Anderson, J.A.R., Muller, J., 1975. Palynological study of a Holocene peat and a Miocene coal deposit from N.W. Borneo. Review of Palaeobotany and Palynology, 19/4, 291–351. https://doi.org/10.1016/0034-6667(75)90049-4

Arutmin, 2015. Internal report on coal mining development of PT Arutmin Indonesia 2015–2020). PT Arutmin Indonesia, Jakarta, 441 pp. (in Indonesian).

Arya, G.C., Sarkar, S., Manasherova, E., Aharoni, A., Cohen, H., 2021. The Plant Cuticle: An Ancient Guardian Barrier Set Against Long-Standing Rivals. Frontiers in Plant Science, 12, 663165. https://doi.org/10.3389/fpls.2021.663165

ASTM, 2012. D3174-2012. Standard Test Method for Ash in the Analysis Sample of Coal and Coke from Coal, 6 pp.

ASTM, 2017. D3173-2017. Standard Test Method for Moisture in the Analysis Sample of Coal and Coke, 4 pp.

Bechtel, A., Gruber, W., Sachsenhofer, R.F., Gratzer, R., Püttmann, W., 2001. Organic geochemical and stable carbon isotopic investigation of coals formed in low-lying and raised mires within the Eastern Alps (Austria). Organic Geochemistry, 32/11, 1289–1310. https://doi.org/10.1016/S0146-6380(01)00101-2

Bechtel, A., Gruber, W., Sachsenhofer, R.F., Gratzer, R., Püttmann, W., 2003a. Depositional environment of the Late Miocene Hausruck lignite (Alpine Foreland Basin): Insights from petrography, organic geochemistry, and stable carbon isotopes. International Journal of Coal Geology, 53, 153–180. https:// doi.org/10.1016/S0166-5162(02)00194-5

Bechtel, A., Sachsenhofer, R.F., Markic, M., Gratzer, R., Lucke, A., Püttmann, W., 2003b. Paleoenvironmental implications from biomarker and stable isotope investigations on the Pliocene Velenje lignite seam (Slovenia). Organic Geochemistry, 34/9, 1277–1298. https://doi.org/10.1016/S0146-6380(03)00114-1

Bechtel, A., Reischenbacher, D., Sachsenhofer, R.F., Gratzer, R., Lücke, A., Püttmann, W., 2007. Relations of petrographical and geochemical parameters in the middle Miocene Lavanttal lignite (Austria). International Journal of Coal Geology, 70/4, 325–349. https://doi.org/10.1016/j.coal.2006.07.002

Bechtel, A., Gratzer, R., Sachsenhofer, R.F., Gusterhuber, J., Lücke, A., Püttmann, W., 2008. Biomarker and carbon isotope variation in coal and fossil wood of Central Europe through the Cenozoic. Palaeogeography, Palaeoclimatology, Palaeoecology, 262/3–4, 166–175. https://doi.org/10.1016/j.palaeo.2008.03.005

Bourbonniere, R.A., Meyers, P.A., 1996. Sedimentary geolipid records of historical changes in the watersheds and productivities of Lakes Ontario and Erie. Limnology and Oceanography, 41/2, 352–359. https://doi.org/10.4319/lo.1996.41.2.0352

BP, 2022. bp Statistical Review of World Energy 2022, 71st edition. https://www.bp.com/content/dam/bp/business-sites/en/global/corporate/pdfs/energy-economics/statistical-review/bp-stats-review-2022-full-report.pdf (accessed on 23 April 2023)

Bray, E.E., Evans, E.D., 1961. Distribution of n-paraffins as a clue to recognition of source beds. Geochimica et Cosmochimica Acta, 22/1, 2–5. https://doi.org/10.1016/0016-7037(61)90069-2

Brooks, J.D., Gould, K., Smith, J.W., 1969. Isoprenoid Hydrocarbons in Coal and Petroleum. Nature, 222, 257–259. https://doi.org/10.1038/222257a0

Buggle, B., Wiesenberg, G.L., Glaser, B., 2010. Is there a possibility to correct fossil n-alkane data for postsedimentary alteration effects? Applied Geochemistry, 25/7, 947–957. https://doi.org/10.1016/j.apgeochem.2010.04.003

Bumi Resources, 2021. Annual Report 2021. http://www.bumiresources.com/index.php/en/investor-relations#report (accessed on 01 January 2023).

Calder, J., Gibling, M., Mukhopadhyay, P.K., 1991. Peat formation in a Westphalian B piedmont setting, Cumberland Basin, Nova Scotia: implications for the maceral-based interpretation of rheotrophic and raised paleomires. Bulletin Societe Geologique de France, 162/2, 283–298.

Cameron, C.C., Esterle, J.S., Palmer, C.A., 1989. The geology, botany and chemistry of selected peat-forming environments from temperate and tropical latitudes. International Journal of Coal Geology, 12/1–4, 105–156. https://doi.org/10.1016/0166-5162(89)90049-9

Casagrande, D.J., 1987. Sulphur in peat and coal. Geological Society, London, Special Publications, 32/1, pp. 87–105. https://doi.org/10.1144/GSL.SP.1987.032.01.07

Dai, S., Bechtel, A., Eble, C.F., Flores, R.M., French, D., Graham, I.T., Hood, M.M., Hower, J.C., Korasidis, V.A., Moore, T.A., Püttman, W., Wei, Q., Zhao, L., O'Keefe, J.M.K., 2020. Recognition of peat depositional environments in coal: A review. International Journal of Coal Geology, 219, 103383. https://doi.org/10.1016/j.coal.2019.103383

Dehmer, J., 1993. Petrology and organic geochemistry of peat samples from a raised bog in Kalimantan (Borneo). Organic Geochemistry, 20/3, 349–362. https://doi.org/10.1016/0146-6380(93)90125-U

Demchuk, T., Moore, T.A., 1993. Palynofloral and organic characteristics of a Miocene bog-forest, Kalimantan, Indonesia. Organic Geochemistry, 20/2, 119–134. https://doi.org/10.1016/0146-6380(93)90032-7

Didyk, B.M., Simoneit, B.R.T., Brassell, S.T., Eglinton, G., 1978. Organic geochemical indicators of palaeoenvironmental conditions of sedimentation. Nature, 272, 216–222. https://doi.org/10.1038/272216a0

Diessel, C.F.K., 1986. The correlation between coal facies and depositional environments. Proceedings of the 20th Symposium of Department Geology, University of New Castle, New South Wales, pp. 11–22.

Ding, L.-F., Liu, J.-X., Xie, Z.-Q., Wang, S.S., Nie, W., Song, L.-D., Wu, X.-D., Zhao, Q.-S., 2019. Magnograndins J-M, elemane sesquiterpenoids from the leaves of Magnolia grandiflora and their inhibitory effects on nitric oxide production. Phytochemistry Letters 31, 121–124. https://doi.org/10.1016/j.phytol.2019.03.021

Espitalie, J., Madec, M., Tissot, B., Mennig, J.J., Leplat, P., 1977. Source Rock Characterization Method for Petroleum Exploration. Offshore Technology Conference. https://doi.org/10.4043/2935-MS

Esterle, J.S., Ferm, J.C., 1994. Spatial variability in modern tropical peat deposits from Sarawak, Malaysia and Sumatra, Indonesia: analogues for coal. International Journal of Coal Geology, 26/1–2, 1–41. https://doi.org/10.1016/0166-5162(94)90030-2

Esterle, J.S., Ferm, J.C., Tie, Y.L., 1989. A test for the analogy of tropical domed peat deposits to "dulling-up" sequences in coal beds-preliminary results. Organic Geochemistry, 14/3, 333–342. https://doi.org/10.1016/0146-6380(89)90060-0

Ettingshausen, C., 1888. Die fossile Flora von Leoben in Steiermark. 1., 2. Theil. - Denkschriften kaiserliche Akademie der Wissenschaften. mathematisch-naturwissenschaftliche Classe, 54, 261–318, 319–384. https://doi.org/10.5962/bhl.title.118927

Ficken, K.J., Li, B., Swain, D., Eglinton, G., 2000. An n-alkane proxy for the sedimentary input of submerged/floating freshwater aquatic macrophytes. Organic Geochemistry, 31/7–8, 745–749. https://doi.org/10.1016/S0146-6380(00)00081–4

Figueiral, I., Mosbrugger, V., Rowe, N.P., Ashraf, A.R., Utescher, T., Jones, T.P., 1999. The Miocene peat-forming vegetation of northwestern Germany: an analysis of wood remains and comparison with previous palynological interpretations. Review of Palaeobotany and Palynology, 104/3–4, 239–266. https://doi.org/10.1016/S0034-6667(98)00059-1

Fikri, H.N., Sachsenhofer, R.F., Bechtel, A., Gross, D., 2022a. Organic geochemistry and petrography in Miocene coals in the Barito Basin (Tutupan Mine, Indonesia): Evidence for astronomic forcing in kerapah type peats. International Journal of Coal Geology, 256, 103997. https://doi.org/10.1016/j.coal.2022.103997

Fikri, H.N., Sachsenhofer, R.F., Bechtel, A., Gross, D., 2022b. Coal deposition in the Barito Basin (Southeast Borneo): The Eocene Tanjung Formation compared to the Miocene Warukin Formation. International Journal of Coal Geology, 263, 104117. https://doi.org/10.1016/j.coal.2022.104117

Friederich, M.C., Moore, T.A., Flores, R.M., 2016. A regional review and new insights into SE Asian Cenozoic coal-bearing sediments: why does Indonesia have such extensive coal deposits? International Journal of Coal Geology, 166, 2–35. https://doi.org/10.1016/j.coal.2016.06.013

Gruber, W., Sachsenhofer, R.F., 2001. Coal deposition in the Noric Depression (Eastern Alps): raised and low-lying mires in Miocene pull-apart basins. International Journal of Coal Geology, 48/1–2, 89–114. https://doi.org/10.1016/S0166-5162(01)00049-0

Hall, R., 2012. Late Jurassic-Cenozoic reconstructions of the Indonesian region and the Indian Ocean. Tectonophysics, 570–571, 1–41. https://doi.org/10.1016/j.tecto.2012.04.021

Hall, R., Morley, C.K., 2004. Sundaland basins. In: Clift, P., Wang, P., Kuhnt, W., Hayes, D.E. (eds.), Continent-Ocean Interactions within the East Asian Marginal Seas. Geophysical Monograph Series, 149, American Geophysical Union, Washington, D.C., 55–85. https://doi.org/10.1029/149GM04

Hauke, V., Graff, R., Wehrung, P., Trendel, J.M., Albrecht, P., Riva, A., Hopfgartner, G., Gülaçar, F.O., Buchs, A., Eakin, P.A., 1992. Novel triterpene-derived hydrocarbons of the arborane/fernane series in sediments: Part II. Geochimica et Cosmochimica Acta, 56/9, 3595–3602. https://doi.org/10.1016/0016-7037(92)90405-8

Hower, J.C., O'Keefe, J.M., Eble, C.F., Raymond, A., Valentim, B., Volk, T.J., Richardson, A.R., Satterwhite, A.B., Hatch, R.S., Stucker, J.D., Watt, M.A., 2011a. Notes on the origin of inertinite macerals in coal: evidence for fungal and arthropod transformations of degraded macerals. International Journal of Coal Geology, 86/2–3, 231–240. https://doi.org/10.1016/j.coal.2011.02.005

Hower, J.C., O'Keefe, J.M., Eble, C.F., Volk, T.J., Richardson, A.R., Satterwhite, A.B., Hatch, R.S., Kostova, I.J., 2011b. Notes on the origin of inertinite macerals in coals: Funginite associations with cutinite and suberinite. International Journal of Coal Geology; 85/1, 186–190. https://doi.org/10.1016/j.coal.2010.11.008

Hutchison, C.S., 1989. Geological evolution of South-East Asia, Oxford Monographs on Geology and Geophysics, 13. Oxford University Press, Oxford, 368 pp.

Hutchison, C.S., 2014. Tectonic evolution of Southeast Asia. Geological Society of Malaysia Bulletin, 60, 1–18. https://doi.org/10.7186/bgsm60201401

ICCP (International Committee for Coal and Organic Petrology), 1998. The new vitrinite classification (ICCP System 1994). Fuel, 77/5, 349–358. https://doi.org/10.1016/S0016-2361(98)80024-0

ICCP (International Committee for Coal and Organic Petrology), 2001. The new inertinite classification (ICCP System 1994). Fuel, 80/4, 459–471. https://doi.org/10.1016/S0016-2361(00)00102-2

IEA, 2022. World Energy Outlook 2002. International Energy Agency. https://iea.blob.core.windows.net/assets/830fe099-5530-48f2-a7c1-11f35d510983/WorldEnergyOutlook2022.pdf (accessed on 09 February 2023)

Jiménez-Moreno, G., Fauquette, S., Suc, J.-P., 2008. Vegetation, climate and palaeoaltitude reconstructions of the Eastern Alps during the Miocene based on pollen records from Austria, Central Europe. Journal of Biogeography, 35/9, 1638–1649. https://doi.org/10.1111/j.1365-2699.2008.01911.x

Korasidis, V.A., Wallace, M.W., Wagstaff, B.E., Holdgate, G.R., Tosolini, A.-M.P., Jansen, B., 2016. Cyclic floral succession and fire in a Cenozoic wetland/peatland system. Palaeogeography, Palaeoclimatology, Palaeoecology, 461, 237–252. https://doi.org/10.1016/j.palaeo.2016.08.030

Kovar-Eder, J., Kcacek, Z., Teodoridis, V., Mazouch, P., Collinson, M.E., 2022. Floristic, vegetation and climate assessment of the early/middle Miocene Parschlug flora indicates a distinctly seasonal climate. Fossil Imprint, 78/1, 80–144. https://doi.org/10.37520/fi.2022.005

Markic, M., Sachsenhofer, R.F., 1997. Petrographic composition and depositional environments of the Pliocene Velenje lignite seam (Slovenia). International Journal of Coal Geology, 33/3, 229–254. https://doi.org/10.1016/S0166-5162(96)00043-2

Moore, T.A., Shearer, J.C., 1997. Evidence for aerobic degradation and implications for Palangka Raya peat sustainability. In: Rieley, J.O., Page, S.E. (eds.), Biodiversity and Sustainability of Tropical Peatlands. Samara Publishing, Cardigan, United Kingdom, 157–167.

Moore, T.A., Shearer, J.C., 2003. Peat/coal type and depositional environment - are they related? International Journal of Coal Geology, 56/3–4, 233–252. https://doi.org/10.1016/S0166-5162(03)00114-9

Moore, T.A., Shearer, J.C., Miller, S.L., 1996. Fungal origin of oxidised plant material in the Palangkaraya peat deposit, Kalimantan Tengah, Indonesia: Implications for 'inertinite' formation in coal. International Journal of Coal Geology, 30/1–2, 1–23. https://doi.org/10.1016/0166-5162(95)00040-2

Morley, R.J., 2012. A review of the Cenozoic climate history of Southeast Asia. In: Gower, D., Johnson, K., Richardson, J., Rosen, B., Rüber, L., Williams, S. (eds.), Biotic Evolution and Environmental Change in Southeast Asia. Cambridge University Press, Cambridge, 79–114. https://doi.org/10.1017/CBO9780511735882.006

Morley, R.J., 2013. Cenozoic ecological history of South East Asian peat mires based on the comparison of coals with present day and Late Quaternary peats. Journal of Limnology, 72/S2, 36–59. https://doi.org/10.4081/jlimnol.2013.s2.e3

Naafs, B.D.A., Inglis, G.N., Blewett, J., McClymont, E.L., Lauretano, V., Xie, S., Evershed, R.P., Pancost, R.D., 2019. The potential of biomarker proxies to trace climate, vegetation, and biogeochemical processes in peat: A review. Global and Planetary Change, 179, 57–79. https://doi.org/10.1016/j.gloplacha.2019.05.006

Otto, A., Wilde, V., 2001. Sesqui-, di-, and triterpenoids as chemosystematic markers in extant conifers - A Review. The Botanical Review, 67/2, 141–238.

Page, S., Rieley, J.O., Shotyk, O.W., Weiss, D., 1999. Interdependence of peat and vegetation in a tropical peat swamp forest. Philosophical Transactions of The Royal Society B - Biological Sciences, 354/1391, 1885–1897. https://doi.org/10.1098/rstb.1999.0529

Page, S., Wüst, R., Banks, C., 2010. Past and present carbon accumulation and loss in Southeast Asian peatlands. PAGES News, 18/1, 25–27. https://doi.org/10.22498/pages.18.1.25

Parr, S.W., 1928. The Classification of Coal. University of Illinois, Engineering Experiment Station, Bulletin, 180, 1–62.

Peel, M.C., Finlayson, B.L., McMahon, T.A., 2007. Updated world map of the Köppen-Geiger climate classification. Hydrology and Earth System Sciences, 11, 1633–1644. https://doi.org/10.5194/hess-11-1633–2007

Peters, K.E., Moldowan, J. M., 1993. The biomarker guide: interpreting molecular fossils in petroleum and ancient sediments. 363 pp.

Pickel, W., Kus, J., Flores, D., Kalaitzidis, S., Christanis, K., Cardott, B.J., Misz-Kennan, M., Rodrigues, S., Hentschel, A., Hamor-Vido, M., Crosdale, P., Wagner, N., 2017. Classification of liptinite - ICCP System 1994. International Journal of Coal Geology, 169, 40–61. https://doi.org/10.1016/j.coal.2016.11.004

Powell, T.G., McKirdy, D.M., 1973. Relationship between ratio of pristane to phytane, crude oil composition and geological environment in Australia. Nature Physical Science, 243, 37–39. https://doi.org/10.1038/physci243037a0

Poynter, J., Eglinton, G., 1990. Molecular composition of three sediments from Hole 717C: the Bengal Fan. In: Cochran, J.R., Stow, D.A.V., et al. (eds.), Proceedings of the Ocean Drilling Program, Scientific Results, College Station, TX (Ocean Drilling Program), 116, 155–161. https://doi.org/10.2973/odp.proc.sr.116.151.1990

Pubellier, M., Morley, C.K., 2014. The basins of Sundaland (SE Asia): Evolution and boundary conditions. Marine and Petroleum Geology, 58/Part B, 555–578. https://doi.org/10.1016/j.marpetgeo.2013.11.019

Radke, M., Schaefer, R.G., Leythaeuser, D., Teichmüller, M., 1980. Composition of soluble organic matter in coals: relation to rank and liptinite fluorescence. Geochimica et Cosmochimica Acta, 44/11, 1787–1800. https://doi.org/10.1016/0016-7037(80)90228-8

Sachsenhofer, R.F., 2000. Geodynamic controls on deposition and maturation of coal in the Eastern Alps. In: F. Neubauer, V. Höck (eds.), Aspects of Geology in Austria, Mitteilungen der Österreichischen Geologischen Gessellschaft, 92, 185–194.

Sachsenhofer, R.F., Bechtel A., Reischenbacher D., Weiss A., 2003. Evolution of lacustrine systems along the Miocene Mur-Mürz fault system (Eastern Alps) and implications on source rocks in pull-apart basins. Marine and Petroleum Geology, 20/2, 83–110. https://doi.org/10.1016/S0264-8172(03)00018-7

Sapiie, B., Rifiyanto, A., 2017. Tectonics and Geological Factors Controlling Cleat Development in the Barito Basin, Indonesia. Journal of Engineering & Technological Sciences, 49/3, 322–339. https://doi.org/10.5614/j.eng.technol.sci.2017.49.3.3

Satyana, A.H., Nugroho, D., Surantoko, I., 1999. Tectonic controls on the hydrocarbon habitats of the Barito, Kutei, and Tarakan Basins, Eastern Kalimantan, Indonesia: major dissimilarities in adjoining basins. Journal of Asian Earth Sciences, 17/1–2, 99–122. https://doi.org/10.1016/S0743-9547(98)00059-2

Schwark, L., Zink, K., Lechterbeck, J., 2002. Reconstruction of postglacial to early Holocene vegetation history in terrestrial Central Europe via cuticular lipid biomarkers and pollen records from lake sediments. Geology, 30/5, 463–466. https://doi.org/10.1130/0091-7613(2002)030<0463:ROPTEH>2.0.CO;2

Scotese, C.R., 2000. PALEOMAP Project [DB/OL]. http://www.scotese.com/ (accessed on 03 February 2023).

Stivrins, N., Ozola, I., Galka, M., Kuske, E., Alliksaar, T., Andersen, T.J., Lamentowicz, M., Wulf, S., Reitalu, T., 2017. Drivers of peat accumulation rate in a raised bog: impact of drainage, climate, and local vegetation composition. Mires and Peat, 19, 1–19. https://doi.org/10.19189/MaP.2016.OMB.262

Stock, A.T., Littke, R., Lücke, A., Zieger, L., Thielemann, T., 2016. Miocene depositional environment and climate in western Europe: The lignite deposits of the Lower Rhine Basin, Germany. International Journal of Coal Geology, 157, 2–18. http://dx.doi.org/10.1016/j.coal.2015.06.009

Taylor, G., Teichmüller, M., Davis, A., Diessel, C.F.K., Littke, R., Robert, P., 1998. Organic Petrology. Gebrüder Borntraeger, Berlin. 704 pp.

van Aarssen, B.G.K., Cox, H., Hoogendoorn, N.P., de Leeuw, J.W., 1990. A cadinene biopolymer in fossil and extant dammar resins as a source for cadinanes and bicadinanes in crude oils from South East Asia. Geochimica et Cosmochimica Acta, 54/11, 3021–3031. https://doi.org/10.1016/0016-7037(90)90119-6

van Aarssen, B.G.K. de Leeuw, J.W., Collinson, M., Boon, J.J., Goth, K., 1994. Occurrence of polycadinene in fossil and recent resins. Geochimica et Cosmochimica Acta, 58/1, 223–229. https://doi.org/10.1016/0016-7037(94)90459-6

Weber L., Weiss A., 1983. Bergbaugeschichte und Geologie der österreichischen Braunkohlevorkommen. Archiv für Lagerstättenforschung der Geologischen Bundesanstalt, 4, 1–217.

Widodo, S., Bechtel, A., Komang, A., Püttmann, W., 2009. Reconstruction of floral changes during deposition of the Miocene Embalut coal from Kutai basin, Mahakam delta, East Kalimantan, Indonesia by use of aromatic hydrocarbon composition and stable carbon isotope ratios of organic matter. Organic Geochemistry, 40/2, 206–218. https://doi.org/10.1016/j.orggeochem.2008.10.008

Widodo, S., Oschmann, W., Bechtel, A., Sachsenhofer, R.F., Komang, A., Püttmann, W., 2010. Distribution of sulfur and pyrite in coal seams from Kutai Basin (East Kalimantan, Indonesia): Implications for paleoenvironmental conditions. International Journal of Coal Geology, 81/3, 151–162. https://doi.org/10.1016/j.coal.2009.12.003

Witts, D., Davies, L., Morley, R., 2014. Uplift of the Meratus Complex: Sedimentology, biostratigraphy, provenance and structure. Proceedings Indonesian Petroleum Association 38th Annual Convention & Exhibition, IPA14-G-082

Witts, D., Hall, R., Nichols, G., Morley, R., 2012. A new depositional and provenance model for the Tanjung Formation, Barito Basin, SE Kalimantan, Indonesia. Journal of Asian Earth Sciences, 56, 77–104. https://doi.org/10.1016/j.jseaes.2012.04.022

Wüst, R.A.J., Hawke, M.I., Bustin, R.M., 2001. Comparing maceral ratios from tropical peatlands with assumptions from coal studies: do classic coal petrographic interpretation methods have to be discarded? International Journal of Coal Geology, 48/1–2, 115–132. https://doi.org/10.1016/S0166-5162(01)00050-7

Zahirovic, S., Seton, M., Müller, R.D., 2014. The Cretaceous and Cenozoic tectonic evolution of Southeast Asia. Solid Earth, 5, 227–273. https://doi.org/10.5194/se-5-227-2014

Zech, M., Buggle, B., Leiber, K., Marković, S., Glaser, B., Hambach, U., Huwe, B., Stevens, T., Sümegi, P., Wiesenberg, G., Zöller, L., 2009. Reconstructing Quaternary vegetation history in the Carpathian Basin, SE-Europe, using n-alkane biomarkers as molecular fossils: Problems and possible solutions, potential and limitations. E&G Quaternary Science Journal, 58/2, 148–155. https://doi.org/10.3285/eg.58.2.03

Received: 13.2.2023
Accepted: 16.4.2023
Editorial Handling: Michael Wagreich